

Dipole excitations to bound states in ^{116}Sn and ^{124}Sn

K. Govaert,* F. Bauwens, J. Bryssinck, D. De Frenne, E. Jacobs, and W. Mondelaers
Vakgroep Subatomaire en Stralingsfysica, University Gent, Proeftuinstraat 86, 9000 Gent, Belgium

L. Govor

Russian Research Center "Kurchatov Institute," Moscow, Russia

V. Yu. Ponomarev

Bogoliubov Laboratory of Theoretical Physics, JINR, Dubna, Russia

(Received 22 December 1997)

Dipole transitions to bound states in the Sn nuclei ^{116}Sn and ^{124}Sn have been investigated by means of nuclear resonance fluorescence (NRF) using 12 MeV linearly polarized bremsstrahlung and unpolarized bremsstrahlung with different end point energies (4.1, 7.5, and 10 MeV). The measurements enable the determination in a completely model-independent way of reduced transition probabilities, multiplicities, and parities of the observed transitions. More than 150 new dipole ground state transitions have been identified. The observed dipole strength distribution displays for both isotopes a clear concentration around 6.5 MeV. For about half of the observed dipole excitations parities could be extracted. They all turned out to be $E1$ excitations except for three tentative $M1$ assignments. The NRF results are compared with data from tagged photon scattering experiments and quasiparticle phonon model calculations. [S0556-2813(98)05105-X]

PACS number(s): 23.20.Lv, 25.20.Dc, 27.60.+j

I. INTRODUCTION

In this paper we report on a high resolution study of the electric and magnetic dipole strength distribution in the even Sn isotopes ^{116}Sn and ^{124}Sn . By resonant scattering of real photons the full energy range of bound states up to the neutron emission threshold at about 9 MeV was investigated. The dominant part of the photon scattering cross section measures the component of the excitation which is reached via electric dipole absorption [1]. In spherical nuclei near closed shells the $E1$ strength distribution often displays fine structure. Closely related to our work are the results of tagged photon scattering experiments on $^{\text{nat}}\text{Sn}$ performed by Axel *et al.* in the relevant energy region between about 6 and 9 MeV [2]. These measurements are complementary to our higher resolution nuclear resonance fluorescence (NRF) experiments in which individual states can be resolved. The elastic scattering cross section for $^{\text{nat}}\text{Sn}$ exhibits fine structure with a pronounced maximum at about 6.5 MeV [2]. Such a peak is often called a pigmy resonance in analogy with the $E1$ giant dipole resonance (GDR) which peaks near 15.5 MeV in the Sn nuclei [3]. Analogous pigmy resonances have been observed in a number of other spherical nuclei near closed shells [4–7]. The most prominent cases are those observed in the mass region around the doubly magic nucleus ^{208}Pb [5,8]. Recently a renewed interest in these pigmy resonances has shown up [9–12].

NRF measurements on a number of Sn isotopes make it possible to check whether the presence of a pigmy resonance is a general characteristic of all even-even Sn nuclei and furthermore to identify a possible isotopic dependence of this

feature. From the seven even-even stable Sn isotopes we have chosen for our study the two extreme cases ^{116}Sn and ^{124}Sn which still have a reasonable natural abundance. It is known that the Lorentz line extrapolation of the $E1$ GDR proved to be too rough for the description of the $E1$ strength behavior below the neutron binding energy in spherical even-even nuclei [13]. This approach usually overestimates to some extent the $E1$ strength function at lower energies and cannot explain the observed substructures. In a microscopic description the fine structure and the presence of pigmy resonances have to be explained via the strength which remains at low energy after most of the original unperturbed $1p-1h$ $E1$ strength has been shifted to higher energies due to the strong residual particle-hole interaction forming the GDR.

At low energy strong electric dipole transitions have been identified recently in NRF experiments on ^{116}Sn and ^{124}Sn at about 3.5 MeV [14]. The corresponding 1^- states have large $E1$ ground state strengths of about 1.5 mW.u. and occur at energies close to the sum of the energies of the 2^+ and the 3^- phonons. They were interpreted as the 1^- member of the two-phonon $2^+ \otimes 3^-$ quintuplet. A systematic investigation of the presence of these two-phonon excitations in the whole chain of even-even Sn nuclei is in progress [15].

The semimagic Sn nuclei ($Z=50$) are an interesting mass region to study the $M1$ spin-flip resonance. This resonance can be explained in the shell model by transitions between the occupied and unoccupied members of the spin-orbit partners, which for heavy nuclei also lie at the basis of the determination of the closed shell configurations [16]. Spin-flip excitations have been studied intensively mainly during the last two decades with the help of diverse techniques, including both electromagnetic and hadronic probes (See [17], and references therein). For heavy nuclei the centroid of the observed $M1$ spin-flip strength agreed quite well with the pre-

*Present address: National Superconducting Cyclotron Laboratory, Michigan State University, East Lansing, MI 48824.

diction according to the rule $41A^{-1/3}$ [MeV] which describes the A dependence of the spin-orbit splitting. For the case of the Sn isotopes a large $M1$ strength is expected around 8 MeV corresponding to $1g_{9/2} \rightarrow 1g_{7/2}(\pi)$, $1g_{9/2} \rightarrow 1g_{7/2}(\nu)$, and $1h_{11/2} \rightarrow 1h_{9/2}(\nu)$ spin-flip excitations. In (p, p') experiments on ^{120}Sn and ^{124}Sn an $M1$ resonance has indeed been observed at an energy around 8.5 MeV. Furthermore there was an indication for an additional structure at about 6.8 MeV in ^{124}Sn [18]. In photon scattering experiments on ^{120}Sn using highly polarized tagged photons a total $M1$ strength of $B(M1) \uparrow \cong 8.8\mu_N^2$ was observed, more or less uniformly distributed throughout the investigated energy range between 7.3 and 9.3 MeV [19].

The experiments described in this article were initiated with the intention of using the high resolution NRF technique to investigate the fine structure and fragmentation of the $E1$ and $M1$ strength below the neutron emission threshold. It should be remarked that the NRF technique is especially suited to investigate $E1$ strength. On the other hand, real photons are not the ideal probe to study $M1$ strengths (other probes such as e and p scattering are more suited), not only because real photon absorption is predominantly $E1$ absorption (the $M1$ absorption probability is some 2 orders of magnitude lower), but also the $E1$ branching of the excited 1^+ to possible 1^- or 2^- levels will have a high probability compared to the $M1$ ground state transition probability. The present article focuses mainly on the higher energy region above 4 MeV. The results for the energy region below 4 MeV have already been published [14] and will here only be used to get a deeper insight into the feeding mechanism of low-lying levels in the experiments with the higher end point energies.

II. NUCLEAR RESONANCE FLUORESCENCE METHOD

In resonant photon scattering experiments the well understood electromagnetic interaction allows the extraction of completely model-independent information. The small momentum transfer of real photons makes photon scattering extremely selective in exciting states, mainly by dipole and to a much lesser extent by $E2$ transitions. The high selectivity of the probe is important for the study of the dipole strength distribution in heavy nuclei such as the investigated Sn isotopes in regions with large level densities. In our NRF experiments all $J=1$ states with sufficient ground state transition width are excited simultaneously by using the continuous energy spectrum of a bremsstrahlung source. A high sensitivity is obtained using Ge γ spectrometers with high efficiency and an excellent energy resolution. As a result, the fragmentation and fine structure of dipole strength distributions can be studied.

The relevant formalism of NRF scattering is briefly presented below. For a more extensive discussion we refer to the review articles [20–22]. The photon scattering cross section, integrated over a single resonance, is given by

$$\begin{aligned} \frac{d\sigma(\vec{\gamma}, \vec{\gamma}')}{d\Omega} &= \frac{2J+1}{2J_0+1} \left(\frac{\pi\hbar c}{E_x} \right)^2 \left(\frac{\Gamma_0\Gamma_f}{\Gamma} \right) \frac{W(\theta, \phi)}{4\pi} \\ &= g(\pi\lambda)^2 \left(\frac{\Gamma_0\Gamma_f}{\Gamma} \right) \frac{W(\theta, \phi)}{4\pi}, \end{aligned}$$

where E_x is the excitation energy of the level and $W(\theta, \phi)$ represents the angular distribution. The scattering angle θ is the angle between the incoming and scattered photon. The azimuthal angle ϕ is the angle between the scattering plane (defined by the incoming and scattered photon) and the polarization plane (defined by the electrical field vector and the direction of the incident photon beam). J_0 and J are the spins of the ground state and the excited state. The ground state decay width, the total width, and the decay width are represented by $\Gamma_0, \Gamma, \Gamma_f$. For the case of elastic scattering in which the excited state decays back to the ground state, the cross section is proportional to Γ_0^2/Γ . If the decay to other states can be observed or is known, then the ground state transition width Γ_0 can be determined. The connection between the experimentally determined width Γ_0 and the reduced transition probability $B(\pi, L) \uparrow$ for a transition with multipolarity L and parity π is given by

$$\Gamma_0 = \frac{8\pi(L+1)}{L[(2L+1)!!]^2} \left(\frac{E_x}{\hbar c} \right)^{2L+1} \frac{2J_0+1}{2J+1} B(\pi, L) \uparrow.$$

The spin of the excited state can be determined by measuring the angular distribution $W(\theta)$ of the scattered photons with respect to the incoming unpolarized photon beam. This angular distribution can be described by a sum of even Legendre polynomials [22]. For the case of even-even nuclei with ground state spin $J_0=0$ it is sufficient to measure the scattered radiation at two different angles. The most favorable angles are $\theta=90^\circ$ and $\theta=127^\circ$. The intensity ratio $W(90^\circ)/W(127^\circ)$ amounts to 0.73 for a dipole and 2.28 for a quadrupole transition. The difference between these theoretical values is slightly reduced for the realistic geometries used in the (γ, γ') experiments.

Parity assignments are crucial for the interpretation of the observed dipole excitations. In photon scattering parities can be extracted in a model-independent way by measuring polarization observables. There are in principle two ways to do this: (i) using linearly polarized photons in the entrance channel and measuring the azimuthal asymmetry of the scattered photons [$(\vec{\gamma}, \gamma')$ experiments] and (ii) using unpolarized photons in the entrance channel and measuring the polarization of the scattered photons via Compton polarimetry $(\gamma, \vec{\gamma}')$ experiments.

Here we will restrict ourselves to a discussion of the first technique which was applied in this work. For a linearly polarized bremsstrahlung beam an azimuthal asymmetry of the scattered photons will be observed. In our NRF experiments this asymmetry is measured using a set of four detectors placed at the scattering angle $\theta=90^\circ$ and parallel ($\phi=0^\circ$ or $\phi=180^\circ$) or perpendicular ($\phi=90^\circ$ or $\phi=270^\circ$) to the polarization plane. In the case of magnetic dipole transitions the photons are scattered parallel to the polarization plane, in the case of electric dipole transitions they are scattered perpendicular to the polarization plane. As the photon beam is not completely polarized, the effect is reduced by the degree of polarization of the beam. The observed count rate asymmetry ϵ is the product of the degree of polarization of the beam P_γ and the analyzing power $\Sigma(\theta)$ of the $(\vec{\gamma}, \gamma')$ reaction

$$\epsilon = \frac{N_{\perp} - N_{\parallel}}{N_{\perp} + N_{\parallel}} = P_{\gamma} \sum (\theta)$$

with N_{\perp} and N_{\parallel} the number of photons scattered perpendicular and parallel to the polarization plane. The analyzing power $\sum(\theta)$ is defined as the normalized difference of the angular distributions for the scattering plane perpendicular and parallel to the polarization plane:

$$\sum (\theta) = \frac{W(\theta, \phi = 90^{\circ}) - W(\theta, \phi = 0^{\circ})}{W(\theta, \phi = 90^{\circ}) + W(\theta, \phi = 0^{\circ})}.$$

The analyzing power is maximal for spin cascades 0-1-0 and 0-2-0 at a scattering angle of 90° and amounts to +1 for $E1$ and -1 for $M1$ and $E2$ transitions. See Fig. 2 in Ref. [23].

III. EXPERIMENTAL SETUP AND PROCEDURE

The NRF experiments reported here have been performed at the linearly polarized bremsstrahlung facility at the 15 MeV linac in Gent [23]. Both angular correlations and cross section measurements using unpolarized bremsstrahlung [(γ, γ') experiments] and polarization measurements using linearly polarized bremsstrahlung [$(\vec{\gamma}, \gamma')$ experiments] were carried out. For the $(\vec{\gamma}, \gamma')$ measurements partially linearly polarized “off-axis” bremsstrahlung was used with a beam energy of 12 MeV. Partially polarized bremsstrahlung is obtained by deviating the electron beam slightly off and back to its axis in a vertical or horizontal plane. The electron beam hits a thin bremsstrahlung radiator placed at the beam axis. A collimator placed along the beam axis selects an off-axis part out of the bremsstrahlung cone. The degree of polarization of the photon beam is measured on-line in a polarization monitor consisting of four Si surface barrier detectors, placed at a scattering angle $\theta = 90^{\circ}$ and azimuthal angles $\phi = 0^{\circ}, 90^{\circ}, 180^{\circ},$ and 270° , in which photoprotons from a thin CD_2 foil are measured. This polarization monitor serves at the same time as a photon flux monitor. Switching of the electron beam through a cycle of the four deviation directions (up-down, left-right, down-up, right-left) is governed by the requirement that during each switching cycle the same integrated photon flux has to be obtained for each of the four directions. The (γ, γ') experiments were performed with end point energies of 7.5 and 10.0 MeV. They link up with previous (γ, γ') measurements performed at the bremsstrahlung facility of the 4 MV Dynamitron in Stuttgart in which the low-energy region below about 4 MeV was investigated [14]. A detailed description of the polarized bremsstrahlung facility in Gent can be found in [23].

The high intensity of the electron beam at the 15 MeV linac in Gent enables the investigation of highly enriched isotopes (see Table I), which in many cases are only available in small quantities (typically a few g). This is of particular importance in the $(\vec{\gamma}, \gamma')$ experiments because of the reduced photon flux in this case due to the use of a thin radiator target and the smaller bremsstrahlung yield at off-axis angles. In the $(\vec{\gamma}, \gamma')$ experiments discussed here the average electron current was of the order of $300 \mu\text{A}$, limited by the thermal capacity of the radiator. In the (γ, γ') experiments on the other hand electron currents of the order of 150

TABLE I. Characteristics of the targets and measuring times.

isotope	^{116}Sn	^{124}Sn
chemical composition	metallic	metallic
enrichment	97.4% (2)	96.3% (2)
isotope mass 7.5 MeV bremsstrahlung	2209 mg	2033 mg
^{11}B mass 7.5 MeV bremsstrahlung	739 mg	739 mg
total measuring time	295 h	291 h
isotope mass in 10 MeV bremsstrahlung	1100 mg	1463 mg
^{11}B mass 10 MeV bremsstrahlung	362 mg	390 mg
total measuring time	356 h	390 h
isotope mass in $(\vec{\gamma}, \gamma')$ measurement	4414 mg	4925 mg
^{11}B mass in $(\vec{\gamma}, \gamma')$ measurement	641 mg	846 mg
total measuring time	865 h	669 h

μA were sufficient to generate fluxes of unpolarized bremsstrahlung, which were about an order of magnitude larger than in the $(\vec{\gamma}, \gamma')$ case.

The targets consisted of 20 mm diameter disks of highly isotopically enriched metallic Sn, sandwiched between H_3BO_3 disks of the same diameter. The well known transitions in ^{11}B and ^{16}O [24,25] served as a standard for energy and efficiency calibration in the (γ, γ') measurements. In the $(\vec{\gamma}, \gamma')$ experiments the H_3BO_3 standard was also used but in a relatively smaller amount and in this case only for energy calibration purposes. Details about the Sn targets used in the different experiments can be found in Table I.

The resonantly scattered photons from the NRF target were detected in four hyperpure Ge detectors with an efficiency at 1.33 MeV varying between 40 and 70 % relative to a standard 3 in. \times 3 in. NaI crystal. Their energy resolutions were 1.7 to 1.8 keV full width at half maximum (FWHM) at 1.33 MeV under standard conditions. Two of the detectors were installed permanently at the scattering angle $\theta = 90^{\circ}$ above and below the NRF target. The other two were installed left and right from the NRF target and were moved between the scattering angles $\theta = 90^{\circ}$ [for the $(\vec{\gamma}, \gamma')$ experiments] and $\theta = 127^{\circ}$ [for the (γ, γ') experiments].

To avoid pile-up effects the count rates of the detectors had to be limited to about one tenth of the pulse repetition rate of the accelerator [26]. Therefore a carbon beam hardener was inserted in the photon beam and lead absorbers with a thickness between 2 and 4 cm were placed in front of the detectors [23]. The count rates of the four Ge detectors were in all measurements limited to about 500 Hz, i.e., about one tenth of the repetition rate of 5000 Hz. The total measuring time for each of the experiments can be found in Table I.

IV. RESULTS

A. The (γ, γ') experiments with 7.5 and 10 MeV bremsstrahlung

In these experiments the complete energy range of bound states up to the neutron emission threshold at about 9 MeV could be covered. The neutron separation energy is 9.56 MeV for ^{116}Sn and 8.49 MeV for ^{124}Sn [27].

Figure 1 displays the (γ, γ') spectra of ^{116}Sn and ^{124}Sn for the energy region between 4.2 and 7.0 MeV. The stron-

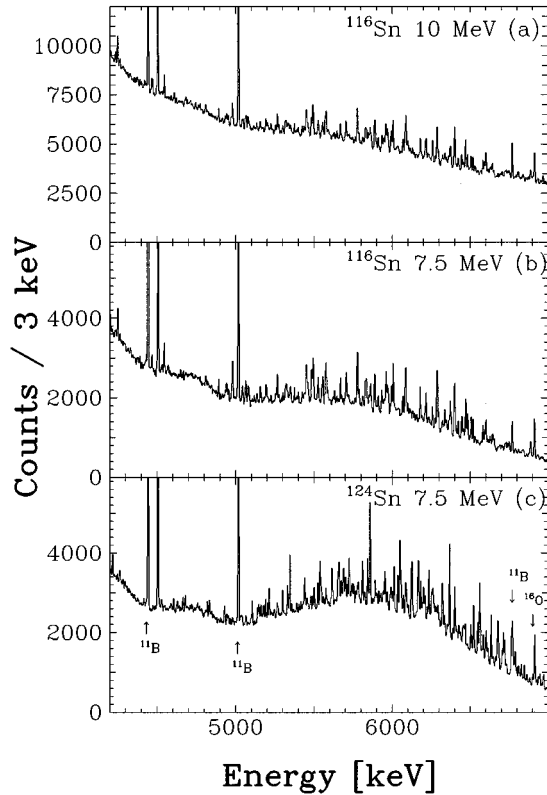


FIG. 1. NRF spectra (a) from ^{116}Sn taken with bremsstrahlung with maximum energy 10.0 MeV and (b) 7.5 MeV and (c) from ^{124}Sn taken with bremsstrahlung with maximum energy 7.5 MeV.

gest lines visible in the spectra below 5.1 MeV, belong to the H_3BO_3 standard. The spectra are quite complex because of the high level density of the Sn isotopes at these high energies and the presence for each transition of the full energy (FE), single escape (SE), and double escape (DE) peaks. In spite of the excellent energy resolution of the Ge detectors (5 to 6 keV at 6 MeV) a number of unresolved multiplets were present in the spectra.

Different criteria were used to accept a line as corresponding to a real transition. In any case at least the FE and SE lines (and if possible also the much smaller DE line) had to be visible in the spectra, both at 90° and 127° . Furthermore, the peak areas of the individual lines had to be in agreement with the known peak ratios FE/SE and FE/DE for the detectors, which had been determined with high precision in calibration measurements on the H_3BO_3 standard. In cases of accidental overlap of lines corresponding to different transitions the observed peak ratios were very helpful.

The analysis of the NRF spectra at lower energies is hindered by the fast increasing background due to the nonresonant interaction of the bremsstrahlung quanta with the NRF target (see Fig. 1). This results in a decrease of the peak to background ratio in the spectra, which for states at too low an energy can lead to the impossibility to determine the spins and parities. These problems can be solved by performing a number of measurements at different bremsstrahlung end point energies. For the investigated Sn isotopes the results of in total three (γ, γ') experiments with an end point energy

of, respectively, 4.1 MeV [23], 7.5, and 10 MeV are now available.

The comparison of the spectra taken with bremsstrahlung with end point energies 10 and 7.5 MeV [see Figs. 1(a) and 1(b)] demonstrates clearly that the background conditions are more favourable in the experiment with the lower end point energy. For the strongest Sn lines around 6.5 MeV the peak to background ratio is about a factor of 3 better in the 7.5 MeV spectrum compared with the 10 MeV spectrum. Furthermore in the 7.5 MeV spectrum there are less problems due to overlapping FE, SE, and DE peaks of different transitions since the energy region of interest is near the end point energy of the measurement. Finally the use of a lower end point energy permits the control of the problem of feeding of low-lying levels from higher lying excited states. In some cases the feeding of low-lying levels can even strongly exceed the direct population of these levels by photoabsorption from the ground state, depending on the end point energy of the bremsstrahlung and the excitation energy of the level in question. Correct results for spins, parities and transitions strengths can only be obtained for levels with an excitation energy not too far away from the end point energy. The feeding phenomenon will be discussed in more detail in Sec. V B.

The excitation energies given in this work are corrected for Doppler and recoil effect. Weighted averages of the energies of all available lines were taken. They are listed in Table II and III. The precision of the excitation energies is in general better than 1 keV.

The spin assignments were based on the ratio of the intensities at scattering angles of 90° and 127° (see Sec. II). In Fig. 2 the measured ratios of the angular distributions $W(90^\circ)/W(127^\circ)$ are shown for all observed ground state transitions in ^{116}Sn . A similar picture is obtained for ^{124}Sn . The full lines at 0.74 and 2.14 represent the expected values for pure dipole and quadrupole scattering. The dashed line represents the situation for the case of an isotropic distribution. All observed ground state transitions above 4.1 MeV both in ^{116}Sn and ^{124}Sn turned out to have a dipole character.

The transition strengths for the observed transitions in the Sn isotopes were determined relative to the well-known reference transitions in the standard isotopes ^{11}B and ^{16}O . The H_3BO_3 standard was irradiated simultaneously with the Sn material using “sandwich” type targets. In this way we avoided the experimental problems of an absolute measurement of the photon flux $N_\gamma(E_x)$ of the bremsstrahlung source. The yields of the reference transitions in the standard allow the determination of $\epsilon_N(E_x) = N_\gamma(E_x) \cdot \epsilon(E_x)$ the product of the photon flux $N_\gamma(E_x)$ and the detector efficiency $\epsilon(E_x)$ (including the effect of the opening angle and the absorption in the lead filter).

In this procedure we make use of the relationship between the integrated photon scattering cross section I_S and the properties of the involved nuclear levels:

$$I_S(E_x) = \int_{4\pi} \frac{d\sigma(\gamma, \gamma')}{d\Omega} d\Omega = \frac{2J+1}{2J_0+1} \left(\frac{\pi \hbar c}{E_x} \right)^2 \frac{\Gamma_0 \Gamma_f}{\Gamma}.$$

The measured peak area A of a line in the NRF spectrum is proportional to the integrated cross section I_S of the (γ, γ') reaction of the level in question via the relation

TABLE II. NRF results for ground state transitions in ^{116}Sn . For states without observed branching, Γ_0 , and the corresponding $B(\pi L)\uparrow$ were calculated under the assumption of pure ground state transitions. Spin and parity assignments in parentheses are tentative. The quoted errors are of statistical nature only.

E_x (keV)	J^π	I_S (eV b)	Γ_0^2/Γ (meV)	Γ_0 (meV)	$B(E1)\uparrow$ ($10^{-3} e^2 \text{ fm}^2$)	Remarks
8739.7 (7)	(1)	55 (10)	364 (67)	364 (67)		
8457.9 (8)	1	39 (9)	242 (55)	242 (55)		
8427.9 (11)	1	67 (13)	413 (80)	413 (80)		
8361.3 (8)	1^-	98 (12)	594 (73)	594 (73)	2.9 (4)	
8282.9 (9)	1	36 (8)	214 (48)	214 (48)		
8247.8 (7)	1	43 (9)	254 (53)	254 (53)		
8234.5 (8)	1	75 (16)	441 (94)	441 (94)		
8214.3 (6)	1^-	148 (10)	866 (60)	866 (60)	4.47 (31)	
8187.4 (7)	1	88 (12)	512 (70)	512 (70)		
7991.6 (8)	1^-	122 (14)	675 (77)	675 (77)	3.8 (4)	
7961.1 (6)	1^-	65 (16)	341 (88)	341 (88)	1.9 (5)	
7947.0 (8)	1	42 (6)	230 (33)	230 (33)		
7933.7 (6)	1	109 (11)	594 (60)	594 (60)		
7925.2 (8)	$1^{(+)}$	101 (23)	544 (123)	544 (123)	0.28 (6)	$B(M1)\uparrow(\mu_N^2)$
7917.1 (7)	1^-	94 (14)	511 (76)	511 (76)	2.9 (4)	
7896.6 (8)	1	155 (21)	838 (115)	838 (115)		
7826.3 (10)	$1^{(-)}$	86 (24)	456 (126)	456 (126)	2.7 (7)	
7758.8 (9)	1	59 (15)	308 (78)	308 (78)		
7654.3 (7)	1^-	135 (35)	685 (175)	685 (175)	4.4 (11)	
7597.8 (10)	1	50 (8)	250 (40)	250 (40)		
7479.8 (14)	$1^{(-)}$	91 (19)	441 (92)	441 (92)	3.0 (6)	a
7353.4 (3)	1^-	98 (9)	460 (38)	460 (38)	3.32 (27)	
7319.9 (7)	1	86 (19)	403 (89)	403 (89)		
7241.4 (6)	1	85 (9)	385 (42)	1030 (120)		b
7235.5 (11)	1	62 (10)	282 (45)	282 (45)		
7215.3 (6)	1	60 (11)	271 (50)	271 (50)		
7203.7 (8)	1	38 (6)	171 (27)	171 (27)		
7165.0 (6)	1	59 (7)	266 (32)	266 (32)		
7154.7 (5)	1^-	88 (8)	390 (35)	390 (35)	3.1 (6)	
7145.8 (6)	1	46 (11)	204 (49)	204 (49)		
7125.6 (5)	1^-	72 (6)	318 (29)	318 (29)	2.5 (4)	
7011.5 (6)	1	44 (7)	187 (29)	380 (50)		b
6967.3 (5)	1	41 (8)	173 (34)	173 (34)		
6889.4 (5)	1^-	115 (11)	473 (45)	473 (45)	4.1 (4)	
6877.0 (7)	1	28 (6)	115 (25)	115 (25)		
6834.1 (3)	1	40 (6)	162(24)	162(24)		
6749.5 (5)	1	60 (9)	237(36)	237(36)		
6741.4 (6)	(1)	44 (8)	173 (31)	173 (31)		
6654.9 (7)	(1)	44 (12)	173 (46)	173 (46)		
6593.2 (5)	1^-	111 (11)	418 (42)	418 (42)	4.2 (4)	
6581.9 (6)	1^-	127 (11)	477 (41)	477 (41)	4.8 (4)	
6518.7 (4)	1^-	109 (10)	402 (37)	512 (51)	5.3 (5)	b
6507.6 (6)	1^-	157 (12)	576 (44)	576 (44)	6.0 (5)	
6484.1 (4)	1^-	150 (13)	551 (47)	551 (47)	5.8 (5)	
6472.3 (3)	1^-	211 (18)	770 (65)	770 (65)	8.1 (7)	
6466.1 (10)	1	69 (18)	254(65)	254 (65)		
6457.2 (5)	1^-	66 (13)	242 (47)	242 (47)	2.6 (5)	
6446.5 (5)	1^-	124 (11)	451 (40)	451 (40)	4.8 (4)	
6423.1 (5)	1^-	91 (9)	326 (32)	454 (48)	4.9 (5)	b
6398.5 (5)	1	135 (15)	479 (54)	479 (54)		
6371.9 (5)	1^-	145 (9)	513 (35)	513 (35)	5.7 (4)	
6363.6 (5)	1	72 (8)	253 (28)	493 (44)		b

TABLE II. (*Continued*).

E_x (keV)	J^π	I_S (eV b)	Γ_0^2/Γ (meV)	Γ_0 (meV)	$B(E1)\uparrow$ ($10^{-3} e^2 \text{ fm}^2$)	Remarks
6339.3 (5)	1^-	111 (10)	390 (38)	390 (38)	4.4 (4)	
6323.0 (6)	1^-	51 (9)	178 (31)	178 (31)	2.0 (4)	
6298.7 (5)	1	86(4)	296 (31)	296 (31)		
6289.0 (4)	1^-	292 (14)	1002 (48)	1002 (48)	11.5 (6)	
6216.7 (5)	1^-	146 (16)	490 (54)	490 (54)	5.8 (6)	
6180.5 (4)	1^-	129 (9)	428 (30)	428 (30)	5.2 (4)	
6088.7 (4)	1	167 (10)	538 (35)	538 (35)		
6083.0 (5)	1	53 (12)	170 (38)	170 (38)		
6006.2 (5)	$1^{(-)}$	124 (12)	388 (38)	388 (38)	5.1 (5)	
5834.7 (5)	1	90 (7)	269 (22)	269 (22)		
5630.2 (5)	1^-	24 (5)	66 (13)	66 (13)	1.06 (21)	
5555.4 (5)	1	48 (6)	128 (16)	128 (16)		
5550.7 (5)	1	37 (6)	99 (16)	99 (16)		
5453.5 (4)	$1^{(-)}$	82 (7)	212 (18)	212 (18)	3.74 (32)	
5391.2 (6)	1	17 (5)	42 (12)	42 (12)		
5085.7 (6)	1	32 (5)	72 (11)	72 (11)		
4980.3 (5)	1	63 (6)	135 (13)	135 (13)		
4892.8 (4)	1^-	29 (4)	60 (8)	60 (8)	1.47 (20)	
4547.1 (4)	1^-	53 (6)	95 (11)	95 (11)	2.90 (33)	
4199.8 (3)	1	48 (4)	73 (6)	73 (6)		

^aOnly observed in the 10 MeV measurement.

^bBranching to other states observed.

$$A(E_x) = I_S(E_x) \cdot N_T \cdot N_\gamma(E_x) \cdot \epsilon(E_x) \cdot W(\theta),$$

where N_T is the number of target nuclei in the photon beam. As a consequence, the elastic transition strength Γ_0^2/Γ of excited levels in the Sn isotopes can be calculated from the measured peak areas, the angular correlations, and the ratio of the number of Sn nuclei and standard isotope nuclei, as both are exposed to the same photon flux.

The main source of systematic errors in this calibration procedure arises from the possibility of unidentified feeding of the reference levels by inelastic transitions from levels at higher energy. For the standard isotope ^{11}B additional calibration measurements have been performed on H_3BO_3 in which also the inelastic transitions were observed. From the known branching ratios of the ^{11}B transitions and the peak areas of the inelastic transitions the fractions of the peak areas due to inelastic transitions from higher lying states could be determined for the reference levels. In determining the product $\epsilon_N(E_x) = N_\gamma(E_x) \cdot \epsilon(E_x)$ from the ^{11}B data, the measured peak areas of the ^{11}B reference transitions have been corrected for the amount due to feeding. For a more extensive discussion of the calibration procedure we refer the reader to [28,29].

The final results of the experiments are listed in Tables II and III. In total more than 150 dipole ground state transitions have been identified above 4.1 MeV. Up to now, most of these were unknown. The resulting dipole strength distributions for ^{116}Sn and ^{124}Sn are displayed in Fig. 3. In both cases one observes in the fine structure of the dipole strength a clear concentration at about 6.5 MeV. The strongest dipole transitions, which are present at these energies, have a strength Γ_0^2/Γ of the order of 1 eV.

The parities given in Tables II and III were determined in the ($\vec{\gamma}, \gamma'$) experiments to be discussed below. Assignments of spins and parities in parentheses are tentative. The tables give the excitation energy E_x , the assigned spin J and parity π , and the integrated photon scattering cross section I_S of the levels in the investigated Sn nuclei. Furthermore the elastic transition strength Γ_0^2/Γ , the ground state decay width Γ_0 , and the corresponding reduced transition probability $B(E1)\uparrow$ or $B(M1)\uparrow$ are also given. The last two quantities were calculated assuming $\Gamma_0/\Gamma=1$ for all levels for which no branching to lower lying excited states was observed. The rapidly increasing continuous background with decreasing energy reduces the sensitivity to detect decay branchings to lower lying excited states. As a result only a small number of sufficiently strong inelastic transitions have been identified in the spectra. In these cases the transition strength $\Gamma_0\Gamma_i/\Gamma$ of the identified inelastic transition has been taken into account in the calculation of the ground state transition width Γ_0 of the level in question. Weak inelastic transitions which fall below the experimental detection limits can of course not be excluded. Therefore the ground state decay widths Γ_0 and the reduced transition probabilities $B(E1)\uparrow$ and $B(M1)\uparrow$ given in the Tables II and III have to be considered to be in fact lower limits of the possibly higher real values.

The results given here have been obtained by a combination of the results of the two measurements with, respectively, 7.5 and 10 MeV bremsstrahlung. Because of the arguments given above it is evident that one should use preferentially the results of the 7.5 MeV measurement at low energies. To construct the final tables the 7.5 MeV results were used below 7 MeV and the 10 MeV results above 7.5

TABLE III. NRF results for ground state transitions in ^{124}Sn . For states without observed branching, Γ_0 , and the corresponding $B(\pi L)\uparrow$ were calculated under the assumption of pure ground state transitions. Spin and parity assignments in parentheses are tentative. The quoted errors are of statistical nature only.

E_x (keV)	J^π	I_S (eV b)	Γ_0^2/Γ (meV)	Γ_0 (meV)	$B(E1)\uparrow$ ($10^{-3} e^2 \text{ fm}^2$)	Remarks
8433.2 (10)	1	69 (9)	424 (53)	424 (53)		
8422.8 (7)	1	80 (8)	495 (51)	495 (51)		
8376.2 (11)	1^-	96 (8)	586 (51)	586 (51)	2.9 (2)	
8350.1 (13)	1	52 (7)	316 (42)	316 (42)		
8269.8 (7)	$1^{(+)}$	95 (8)	564 (45)	564 (45)	0.26 (2)	$B(M1)\uparrow(\mu_N^2)$
8256.9 (9)	1	54 (7)	319 (40)	319 (40)		
8228.9 (6)	1	108 (12)	632 (72)	632 (72)		
8214.3 (12)	1	50 (11)	291 (63)	291 (63)		
8162.2 (8)	1	67 (9)	390 (54)	390 (54)		
8131.7 (15)	1	125 (12)	716 (67)	716 (67)		
8118.8 (8)	1	145 (11)	827 (65)	827 (65)		
8111.8 (16)	1	66 (10)	375 (56)	375 (56)		
7998.9 (9)	1^-	91 (12)	506 (68)	506 (68)	2.8 (4)	
7957.1 (9)	1	156 (10)	857 (56)	857 (56)		
7939.0 (12)	1	52 (8)	282 (46)	282 (46)		
7913.1 (8)	1	81 (16)	442 (89)	442 (89)		
7905.1 (12)	1	54 (12)	294 (62)	294 (62)		
7880.2 (5)	1^-	219 (15)	1181 (80)	1181 (80)	6.9 (5)	
7872.1 (6)	1	108 (17)	582 (89)	582 (89)		
7863.4 (8)	1^-	94 (12)	506 (64)	506 (64)	3.0 (4)	
7815.3 (5)	1^-	249 (18)	1321 (95)	1321 (95)	7.9 (6)	
7788.3 (5)	1	111 (13)	582 (66)	582 (66)		
7778.1 (9)	1	56 (12)	294 (63)	294 (63)		
7770.6 (6)	1	80 (15)	420 (79)	420 (79)		
7759.1 (4)	1^-	142 (13)	741 (68)	741 (68)	4.5 (4)	
7747.4 (7)	1^-	115 (12)	598 (63)	598 (63)	3.7 (4)	
7702.6 (9)	1	41 (10)	212 (50)	212 (50)		
7691.2 (7)	1	83 (14)	424 (72)	424 (72)		
7683.9 (11)	1^-	97 (18)	496 (91)	496 (91)	3.1 (6)	
7678.8 (14)	1	54 (11)	274 (58)	274 (58)		
7666.0 (7)	1	47 (8)	241 (41)	241 (41)		
7642.6 (8)	1^-	74 (14)	374 (73)	374 (73)	2.4 (5)	
7603.7 (8)	1^-	153 (21)	768 (104)	768 (104)	5.0 (7)	
7596.4 (10)	1^-	143 (13)	716 (66)	716 (66)	4.7 (4)	
7575.9 (7)	1^-	96 (12)	476 (60)	476 (60)	3.1 (4)	
7566.9 (10)	1	69 (9)	342 (45)	342 (45)		
7550.9 (6)	1^-	111 (16)	548 (81)	548 (81)	3.6 (5)	
7536.5 (7)	1^-	133 (21)	655 (104)	655 (104)	4.4 (7)	
7487.6 (7)	1^-	130 (17)	633 (82)	633 (82)	4.3 (6)	
7394.5 (4)	1^-	103 (17)	488 (79)	488 (79)	3.5 (6)	
7344.4 (7)	1	92 (18)	430 (84)	430 (84)		
7337.5 (7)	1^-	128 (19)	597 (89)	597 (89)	4.3 (6)	
7326.2 (7)	1	58 (14)	269 (66)	269 (66)		
7308.5 (9)	1	58 (14)	268 (65)	268 (65)		
7295.5 (7)	1^-	156 (12)	720 (55)	720 (55)	5.3 (4)	
7258.6 (10)	1	59 (19)	270 (85)	270 (85)		
7233.8 (8)	1	55 (15)	249 (68)	249 (68)		
7125.7 (7)	1	85 (12)	374 (53)	374 (53)		
7086.5 (7)	1	72 (12)	313 (53)	313 (53)		
7071.1 (8)	1	80 (11)	347 (48)	347 (48)		
7062.2 (9)	1	41 (10)	176 (43)	176 (43)		
7032.5 (7)	1^-	111 (12)	472 (52)	472 (52)	3.9 (4)	

TABLE III. (*Continued*).

E_x (keV)	J^π	I_S (eV b)	Γ_0^2/Γ (meV)	Γ_0 (meV)	$B(E1)\uparrow$ ($10^{-3} e^2 \text{ fm}^2$)	Remarks
7018.0 (8)	1	100 (12)	427 (52)	427 (52)		
6947.5 (8)	1	69 (13)	288 (55)	288 (55)		
6938.9 (8)	1	68 (13)	283 (54)	283 (54)		
6928.2 (8)	(1)	77 (20)	320 (83)	320 (83)		
6902.1 (8)	1^-	98 (12)	404 (50)	404 (50)	3.5 (4)	
6847.1 (8)	1^-	125 (14)	508 (57)	508 (57)	4.5 (5)	
6808.0 (6)	$1^{(+)}$	105 (14)	422 (56)	422 (56)	0.35 (5)	$B(M1)\uparrow(\mu_N^2)$
6790.6 (8)	1^-	160 (19)	639 (76)	639 (76)	5.8 (7)	
6775.6 (8)	1	136 (24)	541 (96)	541 (96)		
6764.2 (8)	1^-	197 (25)	781 (99)	781 (99)	7.2 (9)	
6722.3 (6)	1	177 (18)	693 (75)	693 (75)		
6713.6 (7)	1^-	227 (21)	883 (86)	883 (86)	8.3 (8)	
6705.4 (8)	1^-	121 (17)	471 (66)	471 (66)	4.5 (6)	
6683.3 (8)	1^-	165 (21)	639 (85)	639 (85)	6.1 (8)	
6677.9 (7)	1^-	280 (23)	1083 (89)	1083 (89)	10.4 (9)	
6635.6 (6)	1^-	307 (23)	1171 (88)	1171 (88)	11.4 (9)	
6599.8 (7)	1	94 (20)	335 (76)	335 (76)		
6584.1 (6)	1^-	161 (17)	605 (64)	605 (64)	6.0 (6)	
6565.8 (8)	1	143 (18)	534 (67)	534 (67)		
6560.8 (7)	1^-	348 (31)	1299 (116)	1299 (116)	13.1 (12)	
6548.5 (5)	1	188 (20)	699 (74)	699 (74)		
6524.0 (5)	1^-	219 (25)	808 (92)	808 (92)	8.3 (9)	
6503.2 (6)	1	99 (16)	363 (59)	363 (59)		
6467.5 (6)	1	132 (12)	478 (44)	478 (44)		
6453.1 (7)	1	97 (12)	350 (44)	350 (44)		
6369.1 (7)	1^-	469 (27)	1650 (95)	1650 (95)	18.2 (11)	
6321.6 (7)	1^-	189 (17)	654 (59)	654 (59)	7.4 (7)	
6287.1 (7)	1	88 (14)	301 (48)	301 (48)		
6236.5 (7)	1	211 (19)	711 (65)	711 (65)		
6184.0 (6)	1^-	147 (17)	487 (57)	487 (57)	5.9 (7)	
6170.8 (12)	1	133 (13)	439 (43)	439 (43)		
6129.0 (7)	1	171 (18)	557 (59)	557 (59)		
6002.0 (7)	1	86 (13)	268 (41)	268 (41)		
5968.4 (7)	1	68 (12)	210 (37)	210 (37)		
5951.7 (7)	1	108 (15)	331 (46)	331 (46)		
5902.5 (7)	1	28 (10)	85 (31)	85 (31)		
5869.7 (8)	(1)	30 (6)	90 (18)	90 (18)		
5842.5 (7)	1^-	151 (12)	446 (36)	446 (36)	6.4 (5)	
5064.7 (7)		29 (6)	65 (14)	65 (14)		
4953.7 (7)	1	15.5 (31)	33 (7)	33 (7)		
4605.7 (6)		25 (6)	45 (11)	45 (11)		
4263.4 (6)	1	12.4 (18)	19.5 (30)	19.5 (30)		
4219.1 (6)	1	22.6 (24)	34.9 (37)	34.9 (37)		

MeV. In the energy region between 7 and 7.5 MeV the results of the measurements with 7.5 and 10 MeV end point bremsstrahlung agreed well. For this energy region average values of the transition strengths obtained from both (the 7.5 and the 10 MeV) spectra are given.

Below 4.1 MeV a number of transitions were also observed, but due to the strong feeding of these low-lying levels from higher lying excited states for almost all of them no conclusions about multipolarity were possible and the ob-

tained transition strengths were used only in the investigation of the feeding problem (see Sec. V B). The strong feeding of these levels results not only in an overestimation of the real strengths (see Table IV), sometimes very severely, but also hinders the determination of spins and parities. Indeed, in the case of dominant feeding of a level the angular distribution of the scattered photons becomes isotropic and in addition the azimuthal asymmetry in the $(\vec{\gamma}, \gamma')$ experiments is strongly reduced (see Figs. 2 and 4).

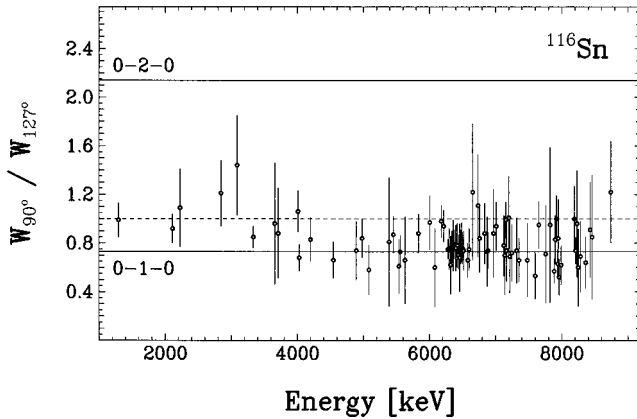


FIG. 2. Ratios of the angular distributions $W(90^\circ)/W(127^\circ)$ for ground state transitions in ^{116}Sn .

B. $(\vec{\gamma}, \gamma')$ experiments with 12 MeV linearly polarized bremsstrahlung

Parity assignments are crucial for the complete characterization of nuclear states. Therefore $(\vec{\gamma}, \gamma')$ experiments with bremsstrahlung with an end point energy of 12 MeV have been performed for both isotopes. In these measurements the excitation by linearly polarized photons leads to an azimuthal asymmetry in the angular distribution of the scattered photons, containing the parity information. For each detector two spectra were recorded, one with the electric field vector of the incident polarized photon beam perpendicular to the scattering plane and the other one with the electric field vector parallel to the scattering plane. The photon flux induced switching procedure of the polarization directions ensures that the effective photon flux is identical in both spectra (see Sec. III and [23]). As a result the azimuthal asymmetry can immediately be extracted from the peak areas in the two

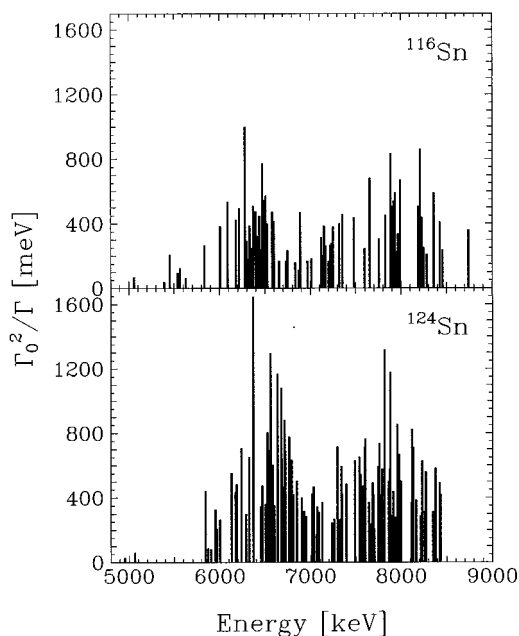


FIG. 3. Dipole strength distribution for ground state transitions in ^{116}Sn and ^{124}Sn above 5 MeV obtained in our NRF experiments.

spectra and is furthermore independent of all detector characteristics. The final asymmetry of a transition is the weighted average for the four detectors.

Figure 4 displays the measured azimuthal asymmetries for ground state transitions in ^{116}Sn . To avoid overloading the figure, only the asymmetries for the strongest transitions are shown for energies above 6 MeV. The dashed bands in the figure represent the expected asymmetry values for electric and magnetic dipole transitions. These values are equivalent to the degree of polarization of the bremsstrahlung beam because the analyzing power for $E1$ or $M1$ transitions has the value $+1$ or -1 (see Sec. II and [23]). For about half of the observed dipole transitions in ^{116}Sn and ^{124}Sn the parity could be extracted from the measured asymmetry. For the assignment of the parities the following criteria were used. A parity was considered to be certain when the asymmetry value was at least 3 standard deviations (3σ) apart from the expected value for the other parity. A parity was also certain when the asymmetry value was at least 2σ apart from the expected value for the other parity and at the same time at most $\sigma/2$ apart from the expected value for its own parity. On the other hand a parity assignment was tentative when only one of the conditions was met. In all other cases no conclusions about the parity were considered possible. The results of the $(\vec{\gamma}, \gamma)$ experiments are also given in Tables II and III. For ^{116}Sn the $(\vec{\gamma}, \gamma)$ experiments led to a parity assignment for 33 dipole excitations above 4.5 MeV. They all turned out to be $E1$ excitations, except for one tentative $M1$ assignment to the level at 7925 keV. In the case of ^{124}Sn 35 $E1$ and 2 tentative $M1$ transitions could be identified above 4.5 MeV.

In Fig. 4 one can easily observe that at lower energies below about 4.5 MeV measured values for the asymmetry are too low. This is an indication for feeding of these low-lying states from higher lying excited states. The dominating feeding of the levels below about 4 MeV (see Sec. V B) results in almost isotropic angular distributions and hence vanishing asymmetries. In the special case of very strong low-lying excitations, for which the effect of the feeding is relatively small, the effect of the feeding on the asymmetry can be corrected by comparing the transition strengths measured at different end point energies [14]. For the state at 3334 keV in ^{116}Sn both the measured asymmetry value (filled diamond) and the asymmetry value after correcting for feeding (open spot) are plotted in Fig. 4. After this correction a conclusive negative parity assignment for this state was possible. For the strong dipole transition at 3490 keV in ^{124}Sn the same conclusion could be drawn. These particular 1^- transitions could be attributed to two-phonon $2^+ \otimes 3^-$ excitations [14].

The results are summarized in Fig. 5 which displays the reduced transition probabilities for the dipole transitions for which the parity could be determined. The hatched bars correspond to tentative parity assignments. The most intense $E1$ transitions are concentrated around 6.5 MeV. Only one tentative $M1$ assignment of the level at 7925 keV in ^{116}Sn could be made with $B(M1) \uparrow = 0.28(6) \mu_N^2$. The total tentative $M1$ strength in ^{124}Sn amounts to $0.61(11) \mu_N^2$. The total observed $B(E1) \uparrow$ strength for the energy region between 5

TABLE IV. Comparison of the transition strengths measured in the (γ, γ') experiments with bremsstrahlung with end point energies 4.1, 7.5, and 10 MeV. The observed values for the ground state strength Γ_0^2/Γ have not been corrected for feeding from higher lying states.

Nucleus	E_x (keV)	J^π	Γ_0^2/Γ	Γ_0^2/Γ	Γ_0^2/Γ	$R(7.5)^a$	$R(10)^a$
			(meV) 4.1 MeV ^b	(meV) 7.5 MeV	(meV) 10 MeV		
¹¹⁶ Sn	1294	2 ⁺	1.10 (10)	27.8 (20)	231 (19)	25.3 (29)	210 (26)
	2844	2 ⁺	2.37 (26)	8.4 (8)	59 (6)	3.5 (6)	24.9 (37)
	3088	2 ⁺	1.11 (21)	9.5 (15)	38 (2)	8.5 (21)	34.5 (65)
	3334	1 ⁻	84.7 (84)	107 (8)	211 (11)	1.26 (16)	2.49 (28)
	4013	1	8.5 (36)	37.1 (27)	148 (7)	4.4 (19)	17.4 (74)
	4027	1	14.6 (56)	67 (15)	108 (7)	4.6 (20)	7.4 (29)
¹²⁴ Sn	1132	2 ⁺	0.488 (67)	16.8 (18)	89 (9)	34 (6)	179 (19)
	2426	2 ⁺	0.41 (10)	12.2 (12)	56 (3)	30 (8)	140 (36)
	3214	1 ⁺	8.87 (97)	19.9 (22)	32.3 (16)	2.2 (4)	3.64 (43)
	3490	1 ⁻	90.2 (98)	104 (4)	147 (5)	1.15 (13)	1.63 (19)
	3697	1	11.3 (17)	20 (4)	57 (4)	1.77 (44)	5.04 (83)
	3710	2 ⁺	6.6 (10)	11.9 (35)	42 (5)	1.8 (6)	6.4 (12)

$$^a R(x) = (\Gamma_0^2/\Gamma)^x \text{ MeV} / (\Gamma_0^2/\Gamma)^{4.1 \text{ MeV}}$$

^bMeasured in Stuttgart [23].

and 8 MeV amounts to $0.125(13) e^2 \text{ fm}^2$ for ¹¹⁶Sn and to $0.203(21) e^2 \text{ fm}^2$ for ¹²⁴Sn.

V. DISCUSSION

A. Sensitivity of the experiments

The sensitivity of our NRF measurements is an important characteristic when comparing our NRF results with data from tagged photon scattering experiments (Sec. V D) and with predictions of theoretical models (Sec. V E). The experimental detection limits were calculated under the assumption that a peak can be observed in the spectrum when its peak area is larger than at least 3 standard deviations of the underlying background. As the measurements on ¹¹⁶Sn and ¹²⁴Sn were performed under similar conditions, their

limits do not differ very much and only the estimates for the case of dipole ground state transitions in ¹¹⁶Sn will be given here.

Figure 6 displays the experimental detection limits for the (γ, γ') experiment with an bremsstrahlung end point energy of 7.5 MeV. The open bars represent the minimum observable ground state transition strength Γ_0^2/Γ while the filled bars represent the corresponding reduced transition probability $B(M1)\uparrow$. For the case of E1 transitions instead of M1 transitions it suffices to change the unit of the transition probability via the relation $1\mu_N^2 = 0.011 e^2 \text{ fm}^2 \cong 1/100 e^2 \text{ fm}^2$ to obtain the corresponding $B(E1)\uparrow$ limit. For energies above 3 MeV one can verify that the detection limits vary between 0.05 and $0.08\mu_N^2$. In previous (γ, γ') experiments performed in Stuttgart with an end point energy of 4.1 MeV a sensitivity, almost an order of magnitude higher, was

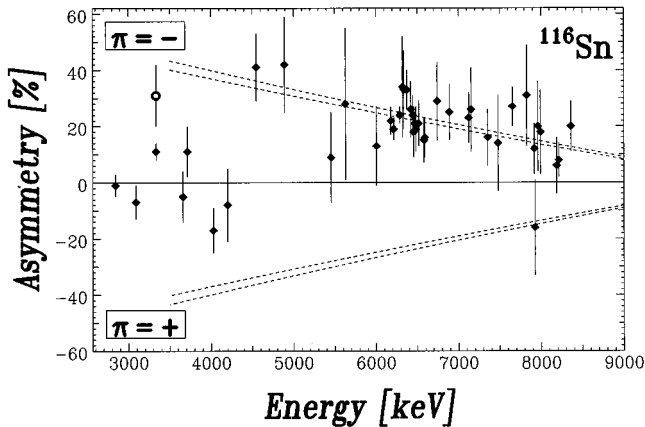


FIG. 4. Asymmetries for ground state transitions in ¹¹⁶Sn. For the 1⁻ state at 3334 keV both the measured value (filled diamond) and the value obtained after correcting for feeding (open circle) are displayed.

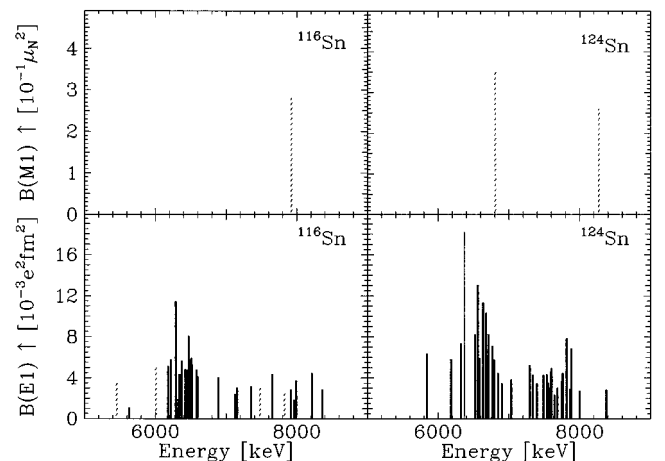


FIG. 5. Distribution of the E1 and M1 strength in ¹¹⁶Sn and ¹²⁴Sn.

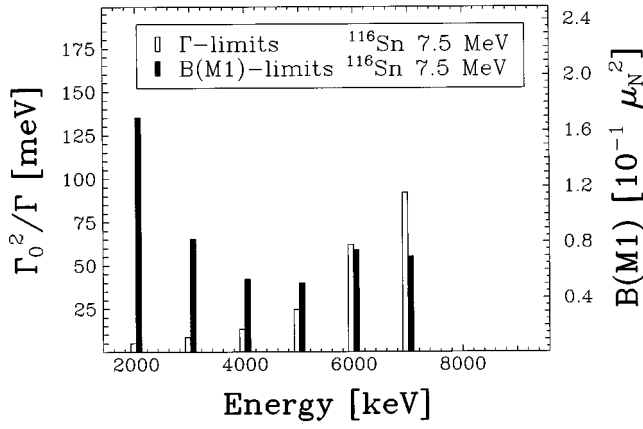


FIG. 6. Experimental detection limits for dipole ground state transitions in ^{116}Sn for the experiment with 7.5 MeV bremsstrahlung.

obtained [14]. The detection limit for the ground state transition strength Γ_0^2/Γ at 3 MeV is about 1 meV in these measurements compared with a value of about 10 meV in the present (γ, γ') measurements with 7.5 MeV bremsstrahlung.

The sensitivities of the (γ, γ') experiments with end point energies of 7.5 and 10 MeV are compared in Fig. 7. The Γ_0^2/Γ detection limits rise fast with increasing energy. In the interesting common energy region between 5 and 7 MeV the detection limits are 60 to 80 % higher in the experiment with 10 MeV bremsstrahlung. This result reflects a less favorable peak to background ratio in the 10 MeV spectrum (see Fig. 1). Note also the drastic change in sensitivity between 7 and 8 MeV when going over from the 7.5 to the 10 MeV measurement.

Despite the longer measuring times, the above limits could not be reached in the $(\vec{\gamma}, \gamma')$ experiments. The higher end point energy in these measurements leads to worse back-

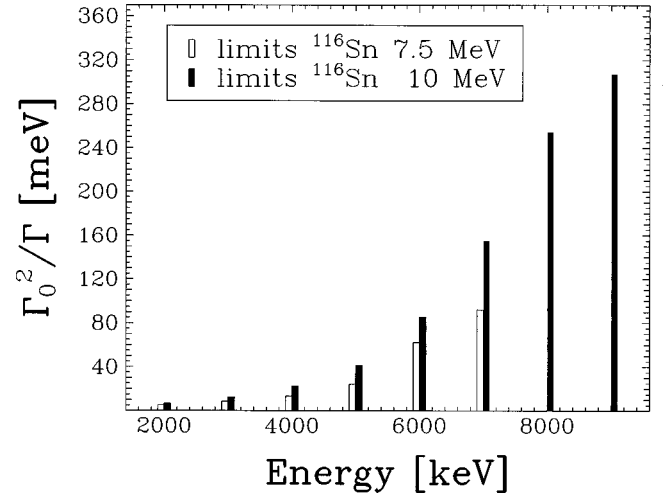


FIG. 7. Comparison of the experimental detection limits for dipole ground state transitions in ^{116}Sn for the experiments with 7.5 MeV and 10 MeV bremsstrahlung.

ground conditions. Analogous calculations lead also to estimates of the limit in the determination of the parity of a dipole ground state transition. This results in a limit for the reduced transition probability $B(M1) \uparrow$ varying from $0.2\mu_N^2$ at 6 MeV to $0.3\mu_N^2$ at 8 MeV, which is two to three times higher than the limit for observing these dipole transitions in the (γ, γ') measurements.

B. Feeding of low-lying levels

An interesting result is obtained by comparing the transition strengths of the levels below 4.1 MeV which could be observed in the three different (γ, γ') experiments with an end point energy of 4.1 [14], 7.5, and 10 MeV (see Sec. IV A). Table IV gives the measured transition strengths Γ_0^2/Γ and their ratios for levels which could be analyzed in

TABLE V. Feeding of low-lying states as a function of the maximum bremsstrahlung energy.

Nucleus	E_x (keV)	J^π	Γ_0 (meV)	Γ_{feed} (meV)	Γ_{feed} (meV)
			4.1 MeV	7.5 MeV	10 MeV
^{116}Sn	1294	2^+	1.10 (10)	26.7 (21)	230 (19)
	2112	2^+		27 (3)	190 (15)
	2225	2^+		12.0 (32)	118 (14)
	2844	2^+	4.02 (44)	11.1 (22)	97 (14)
	3088	2^+	1.71 (33)	12.8 (28)	56 (6)
	3334	1^-	84.7 (84)	22 (11)	126 (14)
	3659	2^+		12.5 (45)	74 (21)
	3712	1		15.5 (33)	101 (38)
^{124}Sn	1132	2^+	0.49 (7)	16.3 (18)	88.5 (91)
	2426	2^+	0.62 (16)	18 (3)	84.2 (79)
	3214	2^+	10.4 (13)	13 (3)	27.5 (27)
	3264	2^+		7.9 (17)	21.6 (28)
	3490	1^-	90.2 (98)	14 (11)	57 (11)
	3697	1	13.3 (21)	11 (6)	54 (6)
	3710	2^+	8.6 (14)	7 (4)	46 (7)
	3762	2^+		10.4 (29)	32 (6)

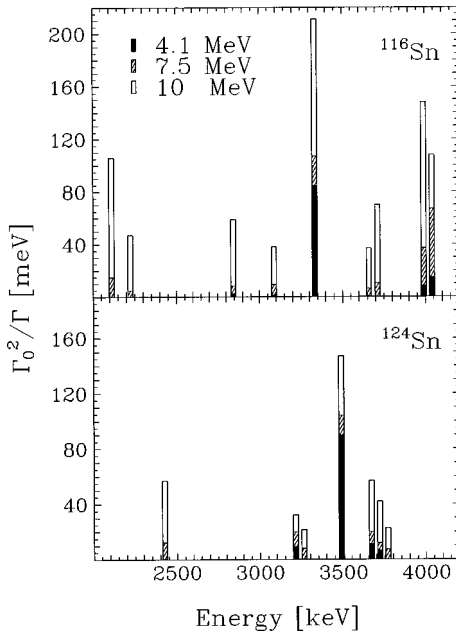


FIG. 8. Comparison of the transition strengths for low-lying levels in ^{116}Sn and ^{124}Sn measured in the experiments with different end point energies.

all three cases, while in Table V the results concerning the feeding in ^{116}Sn and ^{124}Sn are summarized (see further in this section). The spins and parities in Tables IV and V are the result of the NRF measurements in Stuttgart and Gent ([14] and this measurements). For the cases in which only a tentative assignment was possible, the values for spin and parity have been taken from the literature, namely, the compilations for ^{116}Sn [30] and for ^{124}Sn [31] supplemented by the more recent results of $(n, n' \gamma)$ measurements in Moscow for ^{124}Sn [32]. Figure 8 displays for both isotopes the transition strengths Γ_0^2/Γ measured in the three experiments for the energy region between about 2.5 and 4 MeV. It is obvious that the observed transition strengths for all levels increase with increasing end point energy of the measurement.

This phenomenon is expected to be due to the feeding of the low-lying levels in the decay of higher-lying states in the experiments with the higher end point energies. Inelastic transitions, which are responsible for this feeding, were only in a few cases effectively identified in the spectra (see Sec. IV A). The observed inelastic transitions could not explain the differences in measured strengths but only a small part of them. This indicates that the observed feeding proceeds via a large number of weak inelastic transitions, many of which fall below our experimental detection limits.

For most of the levels below 4 MeV the feeding from higher-lying states exceeds the direct population by photoabsorption from the ground state of the nucleus. Indeed, one obtains almost in all cases ratios $R > 2$, even for the measurement with the lower end point energy of 7.5 MeV. Note that a ratio $R > 1$ corresponds with a contribution to the total observed transition strengths which overestimate the real strengths, but also hampers the determination of spins and parities. As already mentioned, in the case of strong feeding unambiguous spin and parity assignments are no longer possible since the angular distributions of the scattered photons become isotropic and the azimuthal asymmetries in the

$(\vec{\gamma}, \gamma')$ experiments vanish (see Figs. 2 and 4).

To investigate the feeding problem we can proceed as follows. The integrated photon scattering cross section for a ground state transition is given by

$$I_s = \frac{2J+1}{2J_0+1} \left(\frac{\pi \hbar c}{E_x} \right)^2 \Gamma_0 \frac{\Gamma_0}{\Gamma}.$$

The feeding of the level from higher-lying states can be accounted for via the following expression for the total observed scattering cross section:

$$I_s = \frac{2J+1}{2J_0+1} \left(\frac{\pi \hbar c}{E_x} \right)^2 (\Gamma_0 + \Gamma_{\text{feed}}) \frac{\Gamma_0}{\Gamma}.$$

The cross section includes now both the direct population of the level by photoabsorption from the ground state (Γ_0) and the indirect population by feeding via inelastic transitions from higher-lying states (Γ_{feed}). One should bear in mind that Γ_{feed} , introduced to describe the contribution due to feeding, is an artificial quantity, which has the same dimension (meV) as the ground state decay width Γ_0 but does not represent a decay width of the level. The ‘‘transition strengths,’’ for lower lying levels ($E_x < 4.1$ MeV) observed in the experiments with end point energies of 7.5 and 10 MeV are to a large and in most cases even for a predominant part ($R > 2$) the result of feeding from higher-lying states. The apparent transition strengths, as given in Table IV, therefore no longer represent the real elastic transition strength Γ_0^2/Γ but in fact the quantity $(\Gamma_0 + \Gamma_{\text{feed}})\Gamma_0/\Gamma$.

Using the known branching ratios Γ_0/Γ for the levels below 4 MeV in ^{116}Sn [30] and ^{124}Sn [31,32] the ground state decay widths Γ_0 can be extracted from the measured transition strengths Γ_0^2/Γ in the experiment with an end point energy of 4.1 MeV [14] and finally also the contribution due to feeding Γ_{feed} from the measured transition strengths $(\Gamma_0 + \Gamma_{\text{feed}})\Gamma_0/\Gamma$ in the experiments with the higher end point energies. These results are compiled in Table V. Furthermore we have also included a number of states which were too weak to be observed in the 4.1 MeV measurements but could be observed in the experiments at higher end point energies due to the strong feeding. For these levels the approximation $\Gamma_0 \ll \Gamma_{\text{feed}}$ was used. This is justified considering the large difference of about an order of magnitude in sensitivity between the (γ, γ') experiments with 4.1 and 7.5 MeV bremsstrahlung (see Sec. V A). Although Γ_{feed} differs from level to level, reflecting the specific nature of each level, there are no drastic fluctuations. In the energy region between 3 and 4 MeV Γ_{feed} varies between about 10 and 20 meV for both isotopes in the 7.5 MeV measurement. At the end point energy of 10 MeV values for Γ_{feed} between about 60 and 120 meV for ^{116}Sn and between about 20 and 60 meV for ^{124}Sn were obtained. The difference between the two isotopes in this case can probably be explained by the difference in neutron emission threshold: 9.56 MeV for ^{116}Sn and 8.49 MeV for ^{124}Sn [27].

The extracted values for Γ_{feed} of both isotopes for the 7.5 MeV measurement are displayed in Fig. 9 together with a least squares fit of the exponential function $\exp[A(1) + A(2)E]$, describing the global decreasing trend of Γ_{feed} with increasing energy. Considering the fluctuations from level to

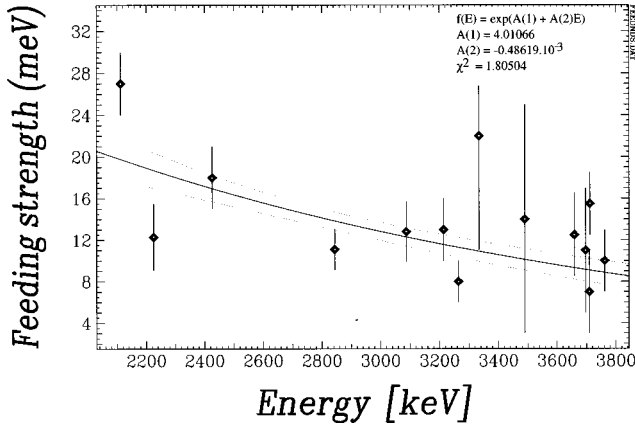


FIG. 9. Energy dependence of the contribution due to feeding Γ_{feed} (see text for meaning) for the measurement with 7.5 MeV bremsstrahlung.

level, a safe estimate of the upper limit of Γ_{feed} of the order of 20 meV at 4 MeV, 10 meV at 5 MeV, and 5 meV at 6 MeV can be reasonably made. As the energy increases, the contribution due to feeding Γ_{feed} decreases, while on the other hand the observed transition strengths Γ_0^2/Γ become larger (see Tables IV and V). In this connection we can repeat that the experimental detection limits for Γ_0^2/Γ rise quickly with increasing energy (see Fig. 7). One can therefore expect that the influence of the feeding on the measured transition strengths will diminish rather rapidly. Using the safe assumption $\Gamma_{\text{feed}} < 20$ meV and taking into account that the observed transition strengths are of the order of 50 to 100 meV in the energy region between 4 and 5 MeV (see Tables II and III), it is clear that feeding cannot be neglected here. For the weakest transitions the real strengths can be overestimated by up to 50%. Above 5 MeV the observed strengths, with the exception of a few weak transitions below about 5.5 MeV, amount to at least 100 meV. For a weak transition corresponding to an observed strength $(\Gamma_0 + \Gamma_{\text{feed}})\Gamma_0/\Gamma$ of only 100 meV, the safe estimates $\Gamma_{\text{feed}} < 10$ meV at 5 MeV and $\Gamma_{\text{feed}} < 5$ meV at 6 MeV lead then on the basis of this worst case scenario assuming a branching ratio $\Gamma_0/\Gamma = 1$ to an overestimation of the real strengths of at most 10% at 5 MeV and 5% at 6 MeV. For the majority of the states, however, the error in the determination of the transition strengths resulting from feeding, will be a lot smaller.

For the levels above 7 MeV the 10 MeV measurement has been used for the extraction of the transition strengths. An analogous estimate of the effect of the feeding at these high energies via an extrapolation of the calculated Γ_{feed} values for energies below 4 MeV from Table V is in this case not appropriate. As an alternative we can compare the transition strengths obtained at 7.5 and 10 MeV. Of importance is the fact that for high energies between 6.5 and 7.5 MeV no systematic higher values could be observed in the 10 MeV measurement. This indicates that the contribution due to feeding in the 10 MeV experiment has already decreased sufficiently at these energies and does not exceed at least the experimental uncertainty on the transition strengths of the stronger transitions, which is of the order of 5 to 10%. Summarizing we can conclude that thanks to the use of several end point en-

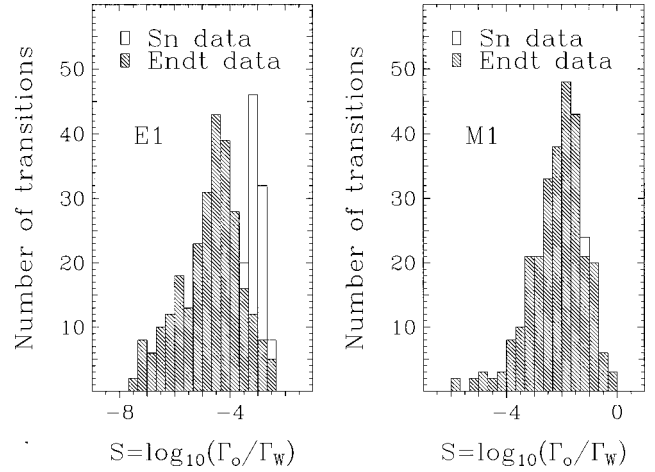


FIG. 10. Distribution of the $E1$ and $M1$ strength in Weisskopf units for the mass region $91 \leq A \leq 150$ (see text).

ergies the influence of feeding on the measured cross sections could be estimated and limited in an acceptable way.

C. Comparison of $E1$ and $M1$ strengths in ^{116}Sn and ^{124}Sn with single particle estimates

The measured $E1$ and $M1$ strengths of the dipole transitions in ^{116}Sn and ^{124}Sn can be compared with the usual transition strengths of electromagnetic transitions in nuclei of this mass region by using single particle Weisskopf estimates. For that purpose it suffices to express the measured $E1$ and $M1$ transition strengths (see Fig. 5) in Weisskopf units (W.u.). In Fig. 10 the distribution of the dipole strength is shown for 273 known $E1$ and 281 known $M1$ transitions for the mass region $91 \leq A \leq 150$, as compiled by Endt [33]. Furthermore the results for the 33 levels in ^{116}Sn and the 37 levels in ^{124}Sn , to which a parity could be assigned, have been included. On the basis of the compilation for the considered mass region, recommended upper limits (RUL) have been deduced by Endt for electric and magnetic transitions of different multiplicities. The RUL amounts to respectively 10 mW.u. for $E1$ transitions and 1 W.u. for $M1$ transitions for the mass region $91 \leq A \leq 150$ [33]. The 68 new $E1$ transitions and the 3 new $M1$ transitions in ^{116}Sn and ^{124}Sn are all within the systematics of the classification (see Fig. 10). The observed $E1$ transitions belong, in comparison with the data from the compilation by Endt, clearly to the stronger transitions. On the basis of the Sn results it is not necessary to raise the RUL for $E1$ transitions for the mass region in question. In the energy region between 6 and 7 MeV 22 (10 in the case of ^{116}Sn and 12 for ^{124}Sn) very strong transitions have been observed with an $E1$ strength larger than 1 mW.u. The strongest excitations at 6289 keV in ^{116}Sn and at 6369 keV in ^{124}Sn have a strength of, respectively, 2.5 and 3.8 mW.u. In NRF experiments on a number of neighboring heavy spherical nuclei, among which are ^{90}Zr [34] and ^{140}Ce [12], similar very strong $E1$ transitions have been observed in the same energy region. The presence of such enhanced $E1$ excitations seems to be a general phenomenon in heavy nuclei near closed shells. It can be explained in the framework of the quasiparticle phonon model (QPM) (Sec. V E).

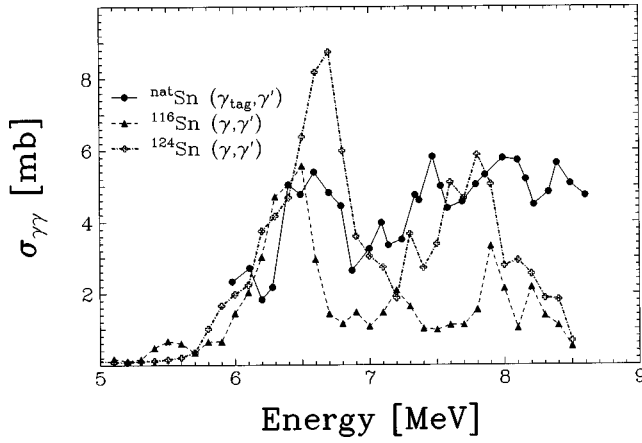


FIG. 11. Comparison of the average elastic photon scattering cross section $\sigma_{\gamma\gamma}$ deduced from our NRF experiments on ^{116}Sn and ^{124}Sn with the result of the tagged photon experiment on $^{\text{nat}}\text{Sn}$ [2].

D. Comparison with results from tagged photon scattering

It is interesting to compare our NRF results for ^{116}Sn and ^{124}Sn with the results of tagged photon scattering experiments on $^{\text{nat}}\text{Sn}$, performed by Axel *et al.* in Urbana, Illinois [2]. In this experiment the elastic photon scattering cross section of $^{\text{nat}}\text{Sn}$ was measured for energies between about 6 and 9 MeV using quasimonochromatic tagged photons with an energy resolution of about 100 keV. This measurement is complementary to our higher resolution NRF experiments in which individual states can be resolved. However, in the NRF measurements one is limited to contributions of sufficiently strong transitions with a strength above the experimental detection limit (see Sec. V A). As a result, part of the total transition strength could not be observed in our measurements and is missing in the NRF results given above. The tagged photon technique, on the other hand, permits the study of the full dipole strength independent of the fragmentation. To compare our NRF results for ^{116}Sn and ^{124}Sn with the data of the tagged photon scattering experiment on $^{\text{nat}}\text{Sn}$, we have extracted from our NRF results for discrete levels (see Tables II and III) an averaged elastic photon scattering cross section by smearing out the measured cross sections I_s of all observed levels above 5 MeV via the Breit-Wigner function

$$\sigma_{\gamma\gamma}(E) = \sum_{\nu} I_{s\nu} \frac{1}{2\pi} \frac{\Delta}{(E - E_{\nu})^2 + \Delta^2/4}.$$

The sum was taken over all observed $J^{\pi} = 1^{-}$ states above 5 MeV. In agreement with the energy resolution of the tagged photon experiment a value $\Delta = 0.1$ MeV has been used. The results are shown in Fig. 11.

The observed elastic photon scattering in the natural Sn experiment is surely dominated by the three most abundant isotopes, namely, ^{116}Sn (14.2%), ^{118}Sn (24.0%), and ^{120}Sn (33.0%). Of course one can expect some variation in the cross sections from isotope to isotope and therefore the result of the tagged photon experiment only represents a lower limit for the fluctuations and substructures, which might exist in the cross sections of individual isotopes.

The elastic photon scattering cross sections in Fig. 11 display fine structure with a pronounced maximum at about

6.5 MeV in all three cases. As mentioned earlier one often labels such a peak ‘‘pigmy resonance’’ in analogy with the $E1$ giant dipole resonance (GDR) which peaks near 15.5 MeV in the Sn nuclei [3]. The pigmy resonance is clearly present in the NRF experiments on ^{116}Sn and ^{124}Sn with a center of gravity at, respectively, about 6.40 and 6.65 MeV. In the tagged photon experiment on $^{\text{nat}}\text{Sn}$ the peak appears at about 6.60 MeV and is somewhat broader. This can be explained by the presence of similar resonances, which can be expected at about the same energy, for the different Sn isotopes. To identify a possible (slight) isotopic dependence of the pigmy resonance position it would be interesting to search for this resonance in at least one of the intermediate nuclei of the Sn isotopic chain. At higher energies above about 7 MeV some more irregularities are present in the cross sections in Fig. 11 but no more clear bumps can be identified.

Analogous pigmy resonances have been observed in a number of other heavy spherical nuclei near closed shells both in NRF measurements and in tagged photon experiments [2,4–8]. They are comprised of ^{90}Zr [2,7], Ba [6], and Ce [6] isotopes and a number of nuclei in the mass region around ^{208}Pb [5,6,8], where the most prominent cases have been observed.

Such a concentration of electric dipole strength in some energy regions below the giant dipole resonance and near 6–7 MeV (pigmy resonance) received increased interest in the last few years [9–11,35]. Iachello suggested that oscillations of a small portion of nuclear matter relative to the rest of the nucleus could be responsible for the observed enhancement of $E1$ strength in certain energy regions well below the $E1$ GDR [35]. This type of oscillation should be present in all nuclei. Van Isacker *et al.* [11] discussed the possibility that nuclei with a reasonable neutron skin could exhibit pigmy- $E1$ resonances below the $E1$ GDR. Heyde *et al.* [10] proposed a schematic two-group random-phase approximation (RPA) model to study the $E1$ strength and its location. They found that the model implies a concentration of local dipole strength in some region of the lower tail of the $E1$ GDR.

Finally we want to perform a quantitative comparison of our results with results obtained in tagged photon experiments. In a first approximation it seems reasonable to assume that all Sn isotopes will have roughly equal cross sections. Because of the higher quality and more in particular the higher sensitivity of the (γ, γ') experiments with 7.5 MeV bremsstrahlung (see Secs. IV A and V A) and because the tagged photon experiment on $^{\text{nat}}\text{Sn}$ starts only at 6 MeV, we will first investigate the energy region between 6 and 7.5 MeV. For this interval the following values for the summed dipole strength have been observed in our NRF experiments: $\sum_i I_{s_i} = \int_6^{7.5} \sigma_{\gamma\gamma}(E) dE = 3.93(48)$ MeV mb for ^{116}Sn and 6.61(80) MeV mb for ^{124}Sn . In the same energy region a transition strength of 5.83(60) MeV mb was observed in the tagged photon experiment on $^{\text{nat}}\text{Sn}$. Final conclusions about the strength, which are missing in our NRF results due to the limited sensitivity of our measurements, can only be made after additional NRF measurements are performed on the isotopes ^{118}Sn and ^{120}Sn , having the largest abundance (together 57%) in the natural isotopic mixture. Nevertheless already now it becomes clear that in the considered energy

region the missing transition strength in our NRF measurements is not very large. At higher energies above 7.5 MeV the difference between the cross sections measured in the NRF experiments and the tagged photon experiment increases fast with increasing energy (see Fig. 11). In the interval between 7.5 and 8.5 MeV 76% for ^{124}Sn and only 34% for ^{116}Sn of the dipole strength observed in the tagged photon experiment can be resolved in our NRF measurements. An analogous comparison of the results for ^{56}Fe , obtained in NRF experiments with a similar sensitivity as our measurements and tagged photon scattering experiments, indicated that in the energy region between 7 and 9 MeV about half of the total dipole strength, measured with tagged photons, could be explained by the strong resonances, observed in the NRF measurements [36].

E. Comparison with QPM calculations

The observed $E1$ strength distribution can in a simple phenomenological approach be described as the extrapolation of the low-energy tail of the $E1$ giant dipole resonance. The energy dependence of the absorption cross section in the GDR can be well described by a resonance line of Lorentz shape:

$$\sigma_{\gamma}(E) = \frac{\sigma_{\text{GDR}}}{1 + (E^2 - E_{\text{GDR}}^2)^2 / E^2 \Gamma_{\text{GDR}}^2}$$

with σ_{GDR} the amplitude, E_{GDR} the excitation energy, and Γ_{GDR} the width of the resonance. The Lorentz line parameters for the even Sn isotopes are $\sigma_{\text{GDR}} \cong 270$ mb, $E_{\text{GDR}} \cong 15.5$ MeV, and $\Gamma_{\text{GDR}} \cong 5.0$ MeV [3].

The Lorentz line extrapolation of the $E1$ GDR below the neutron emission threshold can only give a rough description of the average behavior of the $E1$ strength but not the details. This approach usually overestimates the $E1$ strength function at lower energies and cannot at all explain the observed substructures. A microscopic approach via a shell model calculation is in principle capable of a more complete description. In this case the giant resonance consists of a coherent superposition of particle-hole transitions.

For the investigated isotopes ^{116}Sn and ^{124}Sn a microscopic calculation has been performed in the framework of the quasiparticle phonon model [37]. Excited states in even-even nuclei are treated in this QPM approach as phonons and ‘‘quasibosons.’’ The phonon creation operators are denoted by $Q_{\lambda\mu i}^+$. Multipolarity and projection are indicated by λ and μ . The index i distinguishes between phonons with identical λ , but different excitation energy. The phonon creation operators have a microscopic structure:

$$Q_{\lambda\mu i}^+ = \frac{1}{2} \sum_{\tau} \sum_{jj'}^{n,p} \{ \psi_{jj'}^{\lambda i} [\alpha_j^+ \alpha_{j'}^+]_{\lambda\mu} - (-1)^{\lambda-\mu} \varphi_{jj'}^{\lambda i} [\alpha_{j'} \alpha_j]_{\lambda-\mu} \},$$

where $\alpha_{j,m}^+$, $(\alpha_{j,m})$ denotes creation (annihilation) operators of quasiparticles in the single-particle level $j \equiv |n, l, j\rangle$. Due to the fermion structure of the phonons, they obey quasiboson commuting relations:

$$\begin{aligned} & [Q_{\lambda\mu i}, Q_{\lambda'\mu' i'}^+]_- \\ &= \delta_{\lambda,\lambda'} \delta_{\mu,\mu'} \delta_{i,i'} \frac{1}{2} \sum_{jj'} [\psi_{jj'}^{\lambda i} \psi_{jj'}^{\lambda' i'} - \varphi_{jj'}^{\lambda i} \varphi_{jj'}^{\lambda' i'}] \\ & - \sum_{jj' j_2} \sum_{mm' m_2} \alpha_{jm}^+ \alpha_{j'm'} \{ \psi_{jj_2}^{\lambda i} \psi_{j'j_2}^{\lambda' i'} C_{j'm' j_2 m_2}^{\lambda\mu} C_{jm j_2 m_2}^{\lambda'\mu'} \\ & - (-1)^{\lambda+\lambda'+\mu+\mu'} \varphi_{jj_2}^{\lambda i} \varphi_{j'j_2}^{\lambda' i'} C_{jm j_2 m_2}^{\lambda-\mu} C_{j'm' j_2 m_2}^{\lambda'-\mu'} \}. \end{aligned} \quad (1)$$

The phonon structure, i.e., the coefficients $\psi_{jj'}^{\lambda i}$ and $\varphi_{jj'}^{\lambda i}$ [see Eq. (1)] and the corresponding energies $\omega_{\lambda i}$ are obtained by solving quasiparticle RPA eigenvalue equations (QRPA). The model Hamiltonian includes terms corresponding to an average field for neutrons and protons, monopole pairing, and a residual interaction in a separable form. The QRPA equations yield both collective solutions as well as rather pure two quasiparticle configurations [37].

Starting from the one-phonon states, more complex configurations are constructed, i.e., two-phonon $[Q_{\lambda\mu, i}^+ \otimes Q_{\lambda'\mu', i'}^+]_{JM}$, three phonon $[[Q_{\lambda\mu, i}^+ \otimes Q_{\lambda'\mu', i'}^+]_{J'M'} \otimes Q_{\lambda''\mu'', i''}^+]_{JM}$, and multiphonon ones. Finally, the wave function of excited states J^π can be expanded in the same basis, consisting of one-, two-, multiphonon configurations as follows:

$$\begin{aligned} \Psi^\nu(JM) = & \left\{ \sum_{\alpha_1} S_{\alpha_1}^\nu(J) Q_{\alpha_1}^+ + \sum_{\alpha_2 \beta_2} \frac{D_{\alpha_2' \beta_2'}^\nu(J)}{\sqrt{1 + \delta_{\alpha_2, \beta_2}}} \right. \\ & \times [Q_{\alpha_2}^+ Q_{\beta_2}^+]_{JM} + \sum_{\alpha_3 \beta_3 \gamma_3} \frac{T_{\alpha_3' \beta_3' \gamma_3'}^\nu(J)}{\sqrt{1 + \delta_{\alpha_3, \beta_3, \gamma_3}}} \\ & \left. \times [Q_{\alpha_3}^+ Q_{\beta_3}^+ Q_{\gamma_3}^+]_{JM} + \dots \right\} | \rangle_{ph}, \end{aligned} \quad (2)$$

$$\delta_{\alpha_3, \beta_3, \gamma_3} = \delta_{\alpha_3, \beta_3} + \delta_{\alpha_3, \gamma_3} + \delta_{\beta_3, \gamma_3} + 2 \delta_{\alpha_3, \beta_3} \delta_{\alpha_3, \gamma_3},$$

where we limit many-phonon configurations by the three-phonon term in accordance with realistic calculations presented below. By α , β , and γ we mean the combination $\{\lambda, \mu, i\}$ and by α' , β' and γ' the combination $\{\lambda, i\}$. The index $\nu = (1, 2, \dots)$ labels whether a state J^π [Eq. (2)] is the first, second, etc, one in the total energy spectrum of the system. It is assumed that any combination α , β , γ of phonons appears only once. The second and third terms in Eq. (2) include phonons of different multiplicities and parities.

In order to obtain the excitation energies of the states described in Eq. (2) and the coefficients $S_{\alpha_1}^\nu(J)$, $D_{\alpha_2' \beta_2'}^\nu(J)$, and $T_{\alpha_3' \beta_3' \gamma_3'}^\nu(J)$, we diagonalize the QPM Hamiltonian in the basis of the wave function [Eq. (2)]. The interaction matrix elements between different configurations are calculated by making use of the model Hamiltonian and the microscopic fermion structure of the phonons. It should be noted that in the actual calculations we have omitted terms of the model Hamiltonian corresponding to the two-phonon exchange,

which characterize a direct coupling between one- and three-phonon configurations. This is because matrix elements of two-phonon exchange are much weaker than the ones corresponding to one-phonon exchange and which couple two-phonon configurations to one- and three-phonon configurations, the latter denoted by $U_{\beta'}^{\alpha'}(\gamma')$. Thus the model Hamiltonian in terms of phonon operators can schematically be rewritten as

$$H = \sum_{\alpha'} \omega_{\alpha'} Q_{\alpha'}^+ Q_{\alpha'} + \sum_{\alpha', \beta', \gamma'} U_{\beta'}^{\alpha'}(\gamma') Q_{\alpha'}^+ Q_{\beta'}^+ Q_{\gamma'} + H_{\text{Pauli}}, \quad (3)$$

where phonons α' and β' in the second term are coupled to the angular momentum γ' . The last term H_{Pauli} denotes a Pauli correction, which arises from applying exact commuting relations. It is responsible for an energy shift in the many-phonon configurations from the sum of their unperturbed energies and implies a slight renormalization of the interaction matrix elements $U_{\beta'}^{\alpha'}(\gamma')$. For 1^- states this term is the most essential in describing properties of the first level which has the $(2_1^+ \otimes 3_1^-)_{1^-}$ nature.

Diagonalization of the approximate Hamiltonian [Eq. (3)] in the basis of the wave function [Eq. (2)] has been performed. The phonon basis for the calculations contains all natural parity phonons with λ^π from 1^- up to 6^+ , enlarged with the $\lambda^\pi = 1^+$ unnatural parity phonons. Thereby, we include all one-phonon configurations up to an unperturbed energy of 20 MeV. This truncation allows us to take the influence of the 1^- GDR on low-lying 1^- states fully into account and to avoid the phenomenological inclusion of core-polarization effects on the $E1$ effective charge. The density of the more complex multiphonon configurations is rapidly increasing with excitation energy. Thus to make a calculation possible we have to truncate the basis of multiphonon configurations. In the present calculations we included the two- and three-phonon configurations up to the energy of 9.5 MeV, which resulted in about 600 components for the wave function of Eq. (2). Parameters of the residual interaction in the model Hamiltonian have been adjusted in order to reproduce the experimental position of the GDR, to exclude a spurious state for the 1^- levels and to reproduce the collectivity of the vibrations for other multipolarities.

The one-body fermion operator describing the electromagnetic transition can be expanded as an infinite sum of phonon operators [38], making possible a direct γ excitation of multiphonon configurations starting from the ground state. This is true only if RPA ground state correlations are taken into account [39]. It thereby becomes evident that the direct excitation of the two-phonon states will be weak compared to one-phonon states; the same is true comparing the excitation of three- and two-phonon states, etc. Therefore, we fully neglect the matrix elements of transitions involving three-phonon components of the wave functions. The latter configurations are mainly responsible for a redistribution (fragmentation) of $E1$ ($M1$) strength over the many complex states. Since the wave function of excited states mainly consists of one- and two-phonon configurations, an important interference effect results between these two types of configurations. These interference effects are particularly impor-

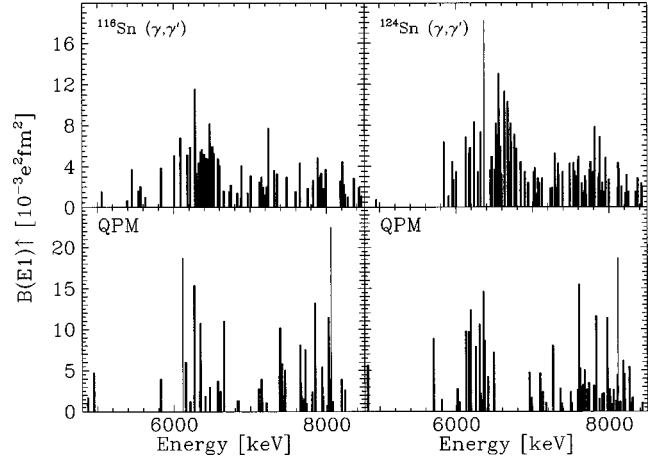


FIG. 12. Comparison of the experimental $E1$ strength for discrete levels in ^{116}Sn and ^{124}Sn with the prediction in the framework of the QPM model.

tant for the lowest lying 1^- states, reducing the $B(E1)\uparrow$ values to the correct order of magnitude compared to the ones found experimentally [14,12]. For the higher-lying 1^- states, the interference exhibits the opposite trend [12]. Making use of the elements discussed above, we have calculated the $B(E1)\uparrow$ and $B(M1)\uparrow$ strength distribution over 1^- and 1^+ states in ^{116}Sn and ^{124}Sn .

In Fig. 12 the experimental $E1$ strength distributions of ^{116}Sn and ^{124}Sn are compared with the theoretical predictions of the QPM calculations. For all observed dipole transitions without parity assignment the reasonable assumption was made that they can be attributed to $E1$ excitation. The overall agreement between theory and experiment is quite good. The experimentally observed fine structure and fragmentation of the $E1$ strength over a large number of individual states and more in particular the presence of a pigmy resonance around 6.5 MeV are reproduced by the QPM calculations. Moreover the theory predicts the appearance of several very strong $E1$ excitations with an $E1$ strength $B(E1)\uparrow > 10^{-2} e^2 \text{ fm}^2$ at these energies (6–6.5 MeV) which have indeed been observed in the experiments. A strong constructive interference between the one- and two-phonon components roughly doubles the $E1$ strength in this energy region relative to the pure one phonon strength. This coherence effect is essential to describe our experimental results and has already been proposed to explain the similar very strong $E1$ transitions which have been observed at about the same energies in NRF experiments on the semimagic $N = 82$ nucleus ^{140}Ce [12]. Moreover the presence of such enhanced $E1$ excitations seems to be a general phenomenon in heavy nuclei near closed shells (see Sec. V C).

Let us now compare the total observed $E1$ and $M1$ strengths with the theoretical predictions. For this comparison we choose to use the energy region between 5 and 8 MeV. Above 8 MeV the rapidly rising limit of sensitivity (see Fig. 7) prevents increasingly the identification of levels, resulting in, for example, the identification of only one state above 8.5 MeV. Below 5 MeV only a few states are observed and feeding in this energy region can no longer be neglected (see Sec. V B). Assuming that all observed dipole transitions have $E1$ character, a total strength of $B(E1)\uparrow$

$=0.204(25) e^2 \text{ fm}^2$ for ^{116}Sn and $B(E1)\uparrow=0.345(43) e^2 \text{ fm}^2$ for ^{124}Sn is obtained. These strengths have to be compared with the predicted values of $B(E1)\uparrow=0.216 e^2 \text{ fm}^2$ for ^{116}Sn and $B(E1)\uparrow=0.229 e^2 \text{ fm}^2$ for ^{124}Sn according to the QPM calculation and $B(E1)\uparrow=0.840 e^2 \text{ fm}^2$ for ^{116}Sn and $B(E1)\uparrow=0.911 e^2 \text{ fm}^2$ for ^{124}Sn according to the Lorentz line extrapolation of the GDR [3]. One should of course bear in mind that the Lorentz line parameters were obtained by fitting of the photoabsorption cross sections which peak about 10 MeV higher than the energy region in question.

On the other hand only one tentative $M1$ excitation to the level at 7925 keV in ^{116}Sn could be observed with $B(M1)\uparrow=0.28(6)\mu_N^2$. In ^{124}Sn the $B(M1)\uparrow$ strength for two observed tentative $M1$ transitions amounts to $0.61(7)\mu_N^2$. The QPM predicts a total $M1$ strength of the order of $B(M1)\uparrow\cong 13\text{--}14\mu_N^2$ for ^{116}Sn and ^{124}Sn with the main strength concentrated at about 9 MeV. In the energy region between 5 and 8 MeV a total $M1$ strength of, respectively, $B(M1)\uparrow=1.52\mu_N^2$ for ^{116}Sn and $B(M1)\uparrow=1.37\mu_N^2$ for ^{124}Sn is predicted by the QPM, corresponding in both cases to less than 10% of the total predicted dipole strength for the considered 5–8 MeV energy region. In agreement with our experimental findings, one can therefore conclude that $M1$ transitions should be difficult to observe in the performed NRF measurements, especially in the case of a strong fragmentation of the $M1$ strength. The lack of $M1$ excitations in our experimental results can be regarded as an indication for a considerable fragmentation of the $M1$ strength over a large number of relatively weak individual transitions which cannot be detected within the sensitivity of our experiments. This is in contrast with our recent NRF experiments on ^{56}Fe and ^{58}Ni , where the number of observed $M1$ transitions almost equals the number of $E1$ transitions [40]. In the considered energy region below 8 MeV the QPM predicts for the strongest $M1$ excitations strengths of the order of $B(M1)\uparrow\cong 0.2\mu_N^2$, which is comparable to the experimental limit for the parity determination (see Sec. V A). Our calculations within the QPM confirm this fragmentation in the energy region under consideration [see Fig. 13(b)] for ^{116}Sn ; the results for ^{124}Sn are very similar.

The quantitative comparison of the experimental $E1$ strength distributions with the theoretical predictions according to either the Lorentz line extrapolation of the GDR or the QPM calculations is, however, hindered by the fact that it is difficult to extract from our NRF results the total strength, including both the full elastic and inelastic components. We are confronted with the following two problems. First of all in NRF measurements one is limited to contributions of sufficiently strong ground state transitions with a transition strength Γ_0^2/Γ above the experimental detection limit. As a result a part of the total transition strength could not be observed in our measurements and is missing in our NRF results. A comparison of our NRF results for ^{116}Sn and ^{124}Sn with the results of tagged photon scattering on $^{\text{nat}}\text{Sn}$ allowed us to check which fraction of the total dipole strength measured with tagged photons could be resolved in our NRF measurements (see Sec. V B). It turned out that in the energy region below 7.5 MeV the missing strength in our NRF measurements is not very large. At higher energies, however, the

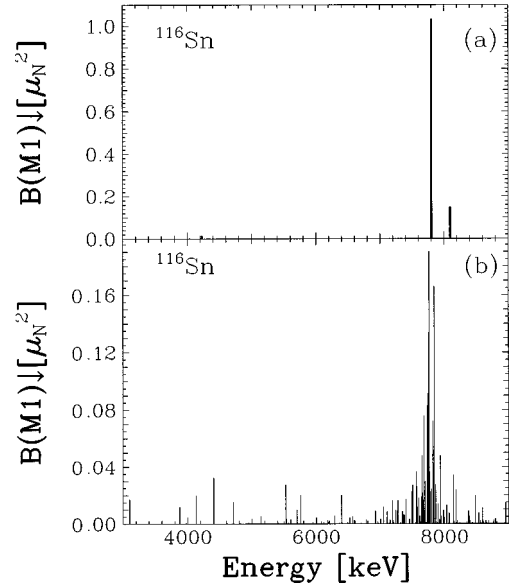


FIG. 13. $M1$ strength distribution in ^{116}Sn over (a) one-phonon states and (b) multiphonon states, Eq. (2).

difference between the cross sections measured in our NRF experiments and in the tagged photon experiment increases fast with increasing energy, indicating that more strength is not detected in our NRF experiment.

The identification of inelastic transitions in NRF measurements poses the second problem. The rapidly increasing background at lower energies in the spectra reduces the sensitivity to detect decay branchings to lower lying excited states. As a result only a small number of sufficiently strong inelastic transitions could be identified in the spectra (see Sec. IV A). The many weak inelastic transitions, responsible for the observed feeding of low-lying levels, fell below our experimental detection limits and could not be observed (see Sec. V B). The reduced transition probabilities $B(E1)\uparrow$ were calculated assuming pure ground state transitions ($\Gamma_0/\Gamma=1$) for all levels for which no branching to lower lying excited states was observed. In the case of a large number of unidentified weak inelastic transitions this can lead to a considerable underestimation of the real strengths.

The total excitation cross sections of high lying states (E_λ) can be represented as a sum of elastic and inelastic cross sections:

$$\begin{aligned} \sigma_{\text{tot}} &= \sigma_{\text{el}} + \sigma_{\text{inel}} \\ &= \sum_{\lambda} (\pi\lambda_{\lambda})^2 g_{\lambda} \frac{\Gamma_{0\lambda}^2}{\Gamma_{\lambda}} + \sum_{\lambda} (\pi\lambda_{\lambda})^2 g_{\lambda} \Gamma_{0\lambda} \sum_i \frac{\Gamma_{i\lambda}}{\Gamma_{\lambda}}. \end{aligned}$$

The second term in this expression describes the feeding of the lower lying states. If for the low-lying excited states (E_i), the excitation cross sections via direct photoabsorption from the ground state and the total feeding of these states are known, then it is possible to estimate the contribution of σ_{inel} and some average total branching ratio $\langle \sum_i B_{\lambda,i} \rangle = \langle \sum_i \Gamma_{\lambda,i} / \Gamma_{\lambda} \rangle$ for inelastic transitions from higher lying states (E_{λ}). This will be explained in more detail in the Appendix. Such an attempt looks very attractive for $^{116,124}\text{Sn}$ as it can be done using only the results of NRF experiments

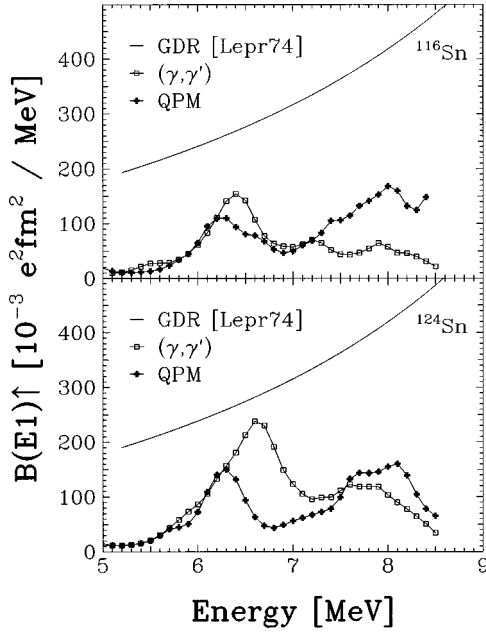


FIG. 14. Comparison of the experimental $E1$ strength distribution in ^{116}Sn and ^{124}Sn with the predictions according to the Lorentz line extrapolation of the GDR and the QPM calculations.

and the known level schemes of these nuclei. It looks also reasonable because the dipole strength is concentrated in the narrow energy region of 6.0–7.0 MeV for the Sn isotopes. We want to stress here that the level scheme below 4 MeV and the branching ratios of gamma transitions from the levels are well known for ^{116}Sn [30,41,42] and (at least the states with $J=1,2^+$) for ^{124}Sn [31,32].

The estimation procedure performed is described in the Appendix. In ^{116}Sn for levels in the region of 5.0–7.4 MeV, the average branching ratio for ground state transitions $\langle \Gamma_{0_\lambda} / \Gamma_\lambda \rangle = 1 - \langle \sum_i \Gamma_{i_\lambda} / \Gamma_\lambda \rangle = 0.54$ is obtained. This value is close to the ratio of $\sigma_{\gamma_0} / \sigma_{\gamma_i} = 0.50$ derived by Axel *et al.* [2] in a statistical approach for the region 6.0–7.5 MeV in the Sn isotopes, using for the excited states some reasonable parameters [the constant sum of partial inelastic radiative widths and the level spacing $D(E)$] obtained in neutron resonance experiments. The branching ratio $\langle \Gamma_{0_\lambda} / \Gamma_\lambda \rangle$ for ^{124}Sn amounts to the higher value 0.72, which correlates with a higher elastic cross section in ^{124}Sn compared to ^{116}Sn (see Fig. 11).

Taking into account the strength missing in our NRF results, both for the elastic and inelastic components, might considerably increase the $E1$ strength. In Fig. 14 we compare the experimental $E1$ strength distributions with the theoretical predictions according to either the Lorentz line extrapolation of the GDR and the QPM calculations. For this comparison we have extracted from our NRF results and the QPM predictions for discrete levels (see Fig. 12) the corresponding $E1$ strength function (in units $e^2 \text{ fm}^2 / \text{MeV}$) by smearing out the reduced transition probabilities $B(E1)\uparrow$ of all observed levels via the Breit-Wigner function

$$B(E1)\uparrow = \sum_{\nu} B(E1, \nu)\uparrow \frac{1}{2\pi} \frac{\Delta}{(E - E_{\nu})^2 + \Delta^2/4}.$$

The sum was taken over all observed dipole states above 5 MeV. So we assumed once more that all dipole transitions are due to $E1$ excitation. The parameter value $\Delta = 0.3$ MeV, applied in the theoretical calculations, has been used for the comparison in Fig. 14. One observes that the QPM predicts considerably less $E1$ strength than what can be expected on the basis of the Lorentz line extrapolation of the GDR. Moreover the strength functions display fine structure with a pronounced bump just above 6 MeV. The pigmy resonance predicted by the QPM calculations in the energy region 6–6.5 MeV has experimentally been observed in both Sn isotopes at slightly higher energies. Finally we want to point out that on the basis of the above extracted average branching ratio of 0.72–0.54 for ground state transitions an additional $B(E1)\uparrow$ strength of 40 to 85 % would show up corresponding to the unobserved inelastic transitions. This would bring the experimental distributions in Fig. 14 somewhere in between the QPM prediction and the GDR extrapolation.

VI. CONCLUSIONS

Via resonant scattering of real photons a high resolution study of the dipole strength distribution in the even Sn isotopes ^{116}Sn and ^{124}Sn has been performed for energies up to the particle threshold at about 9 MeV. A detailed picture of the fine structure of the dipole strength up to these high energies has been obtained. Furthermore the use of linearly polarized bremsstrahlung made possible the determination of the parities of the strongest observed dipole transitions in a completely model-independent way.

More than 150 new dipole ground state transitions in ^{116}Sn and ^{124}Sn were observed. The excitation energies and the ground state transition widths of the corresponding levels have been determined. The observed dipole strength distribution displays for both isotopes a clear concentration around 6.5 MeV, giving rise to a so called pigmy resonance with a total strength of $0.204(25) e^2 \text{ fm}^2$ for ^{116}Sn and $0.345(43) e^2 \text{ fm}^2$ for ^{124}Sn , under the assumption that all observed dipole transitions have $E1$ character. For the strongest transitions parities could be extracted. They all turned out to be $E1$ excitations except for three tentative $M1$ assignments. The most intense $E1$ transitions are concentrated around 6.5 MeV and their transition strengths rise to about 2–3 mW.u. The lack of $M1$ excitations in our experimental results are an indication for a considerable fragmentation of the $M1$ strength over a large number of relatively weak individual transitions which cannot be detected within the sensitivity of our experiments.

By comparing the apparent transition strengths deduced directly from our experiments at different bremsstrahlung end point energies, the conclusion could be drawn that the feeding of lower lying levels can be a rather strong effect. In the extraction of the transition widths this feeding cannot be neglected for levels with an excitation energy much below the bremsstrahlung end point energy. Thanks to the use of bremsstrahlung with different end point energies the influence of the feeding on the measured cross sections could be limited. The error in the determination of the transition strengths resulting from feeding can be estimated to be at most about 10% for excitations above 5 MeV.

Our NRF results for ^{116}Sn and ^{124}Sn as well as the data

from tagged photon scattering experiments on ^{116}Sn indicate that the elastic photon scattering cross sections display fine structure with a pronounced maximum (pigmy resonance) at about 6.5 MeV. Similar resonances can be expected at the same energies in the other Sn isotopes.

The experimental strength distributions are rather well reproduced by QPM calculations taking into account the coupling of up to three phonons. A strong constructive interference between one and two phonon components is essential for the description of the experimental results with in particular the occurrence of very strong $E1$ transitions around 6.5 MeV.

ACKNOWLEDGMENTS

We want to thank the technical staff of the Nuclear Physics Laboratory in Gent for the reliable operation of the linac during the experiments. We thank our long time collaborators Professor U. Kneissl and Dr. H. H. Pitz for their support and advice. The support of Drs. K. Huber, R. D. Heil, A. Jung, S. Lindenstruth, R. Stock, and C. Wesselborg especially in the earlier phase of the experiments is gratefully acknowledged. We are indebted to Professor F. Iachello, Dr. A. Vdovin, Professor K. Heyde, Dr. R. D. Herzberg, and Dr. P. von Neumann-Cosel for stimulating and enlightening discussions and for providing results before publication. This research was supported by the Fund for Scientific Research, Flanders. V. Yu. Ponomarev acknowledges support from the RFBR (Grant No. 96-15-96729).

APPENDIX

The population of low-lying levels in NRF experiments occurs in two different processes: by the direct photoabsorption from the ground state and by cascade transitions from higher lying states. The level population P_i (the number of target nuclei in the state E_i) in this case can be defined as the sum of the population via these two processes:

$$P_i = P_{S_i} + P_{\text{feed}_i} \quad (\text{A1})$$

As a result of the feeding process states with $J^\pi \neq 1^\pm, 2^+$ will be populated in our experiments too, which is confirmed by the observation of inelastic transitions from states with $J^\pi = 0^+$ in the spectra with 10 MeV bremsstrahlung.

The scheme of excited states of ^{116}Sn (and ^{124}Sn) can be separated into the following.

(i) The high-energy region (above about 4.1 MeV). In this region only the ground state transitions are observed in the experiment and the contribution of cascade transitions between these high-lying states is negligible (see Sec. V B). The branching ratios in this region and the complete level scheme are not known. In this energy region the levels will be characterized with an index λ .

(ii) The low-energy region (below about 4.1 MeV, where the levels will be denoted by an index $i, c, \text{ or } m$). In this part of the level scheme the feeding process dominates or gives a considerable contribution in our NRF experiments even with 7.5 MeV maximum bremsstrahlung energy. All the terms in Eq. (A1) can be determined from the experimental data. The P_S values are obtained in our experiment with 4.1 MeV end

point energy bremsstrahlung using known branching ratios. The P_i values are deduced only in the 7.5 MeV measurements. Both ground state transitions and inelastic transitions can be used to find these P_i values.

If $\sum_\lambda P_{S_\lambda} B_{\lambda,i}$ is the population of level i by transitions from all states $E_\lambda > 4.1$ MeV, the total population P_i of level i will be equal to

$$P_i = P_{S_i} + \sum_\lambda P_{S_\lambda} B_{\lambda,i} + \sum_{c=i+1}^L P_c B_{c,i}, \quad (\text{A2})$$

where P_c is the total population (similar to P_i) from a low-lying state c ($E_i < E_c \leq 4.1$ MeV), $B_{c,i}$ is the branching ratio for the transition from level c to state i , and L is the total number of levels with energy below or equal to 4.1 MeV.

For the lowest levels the contribution of the second term can be considerable. For example, for the first 2^+ state in these two Sn isotopes it exceeds 50%.

For the decay of level i we have

$$P_i = P_i B_{i,0} + \sum_{m=1}^{i-1} P_i B_{i,m}, \quad (\text{A3})$$

where $B_{i,0}$ is the branching ratio for a ground state transition, and the index m indicates the states below level i .

The $\sum_\lambda P_{S_\lambda} B_{\lambda,i}$ value can be extracted from Eqs. (A2) and (A3):

$$\sum_\lambda P_{S_\lambda} B_{\lambda,i} = P_i B_{i,0} - P_{S_i} + \left(\sum_{m=1}^{i-1} P_i B_{i,m} - \sum_{c=i+1}^L P_c B_{c,i} \right). \quad (\text{A4})$$

The total feeding for all low-lying states (up to 4.1 MeV) caused by inelastic transitions from levels E_λ is determined as

$$\sum_{i=1}^L \sum_\lambda P_{S_\lambda} B_{\lambda,i} = \sum_{i=1}^L (P_i B_{i,0} - P_{S_i}) + \left(\sum_{i=2}^L P_i \sum_{m=1}^{i-1} B_{i,m} - \sum_{i=1}^{L-1} \sum_{c=i+1}^L P_c B_{c,i} \right). \quad (\text{A5})$$

In each one of the last two terms in Eq. (A5), the total sum accounts for all cascade transitions between low-lying states. The sequence of summation in the last term can be changed to

$$\sum_{i=1}^{L-1} \sum_{c=i+1}^L P_c B_{c,i} = \sum_{c=2}^L P_c \sum_{i=1}^{c-1} B_{c,i}. \quad (\text{A6})$$

This expression does not differ from $\sum_{i=2}^L P_i \sum_{m=1}^{i-1} B_{i,m}$ and we get finally

$$\sum_{i=1}^L \sum_\lambda P_{S_\lambda} B_{\lambda,i} = \sum_{i=1}^L (P_i B_{i,0} - P_{S_i}). \quad (\text{A7})$$

This shows that the total feeding for all low-lying levels (E_i) caused by inelastic transitions from higher-lying levels (E_λ) is equal to the total number of ground state transitions from these low-lying levels with subtraction of the population P_S

of these levels in (γ, γ') reactions via direct photon absorption [see Eq. (A7)]. This conclusion can be derived from a general consideration as well. Every initial excited state in each nucleus decays directly to the ground state or via the ground state transition from any other intermediate state which is the final excited state in a cascade decay. Due to this reason the total number of ground state transitions will be equal to the total number of excited states in the target, independent of the nature of excitation (directly or by feeding from higher lying levels) and of the number of cascade transitions.

According to the introduced definition of Γ_{feed} (see Sec. V B, second equation), we have

$$\sum_{i=1}^L P_i B_{i,0} = \sum_{i=1}^L N_i g_i (\pi \chi_i)^2 (\Gamma_{0_i} + \Gamma_{\text{feed}_i}) \frac{\Gamma_{0_i}}{\Gamma_i} \quad (\text{A8})$$

and

$$\sum_{i=1}^L P_{S_i} = \sum_{i=1}^L N_i g_i (\pi \chi_i)^2 \Gamma_{0_i}, \quad (\text{A9})$$

where g denotes the state spin factor and N is the photon flux (obtained using the Schiff formula).

The left side of Eq. (A7) can also be written as

$$\begin{aligned} \sum_{i=1}^L \sum_{\lambda} P_{S_{\lambda}} B_{\lambda,i} &= \sum_{\lambda} N_{\lambda} g_{\lambda} (\pi \chi_{\lambda})^2 \Gamma_{0_{\lambda}} \frac{\sum_{i=1}^L \Gamma_{i_{\lambda}}}{\Gamma_{\lambda}} \\ &= \left\langle \frac{\sum_{i=1}^L \Gamma_{i_{\lambda}}}{\Gamma_{0_{\lambda}}} \right\rangle \sum_{\lambda} N_{\lambda} g_{\lambda} (\pi \chi_{\lambda})^2 \frac{\Gamma_{0_{\lambda}}^2}{\Gamma_{\lambda}} \\ &= \frac{\langle X \rangle}{1 - \langle X \rangle} \sum_{\lambda} N_{\lambda} g_{\lambda} (\pi \chi_{\lambda})^2 \Gamma_{0_{\lambda}}^2 / \Gamma_{\lambda}, \end{aligned} \quad (\text{A10})$$

where $\langle X \rangle \equiv \langle \sum_{i=1}^L B_{\lambda,i} \rangle = \langle \sum_i \Gamma_{i_{\lambda}} / \Gamma_{\lambda} \rangle$ and $(1 - \langle X \rangle) \equiv \langle \Gamma_{0_{\lambda}} / \Gamma_{\lambda} \rangle$. Introducing the integrated cross section I_S obtained in the experiments at different end point energies, we can deduce

$$\begin{aligned} \sum \sum P_{S_{\lambda}} B_{\lambda,i} &= \frac{\langle X \rangle}{1 - \langle X \rangle} \sum_{\lambda} N_{\lambda} I_{S_{\lambda}} \\ &= \left(\sum_{i=1}^L N_i I_{S_i} \right)_{7.5 \text{ MeV}} \\ &\quad - \left(\sum_{i=1}^L N_i \frac{I_{S_i}}{B_{i,0}} \right)_{4.1 \text{ MeV}}. \end{aligned} \quad (\text{A11})$$

In principle, we need the data for all low-lying states with $J^{\pi} = 1^{\pm}, 2^+$. For a number of these levels, Γ_0 is determined in our experiment with 4.1 MeV bremsstrahlung. The remaining levels have a low value of Γ_0 (Γ_0^2/Γ is below the limit of sensitivity in this experiment). They are not observed in the experiment in Stuttgart and their contribution in the last term of Eqs. (A7) and (A11) is small. The Γ_0 for some of these levels can be taken from Refs. [30,31]. In the population of these low-lying levels the feeding process dominates ($\Gamma_{\text{feed}} \gg \Gamma_0$) in the 7.5 MeV experiment. The population (and I_S values) of the low-lying states missed in the 7.5 MeV experiment can be found with the use of an average dependence of P_i on the excitation energy. As a rule these levels occur above 3.5 MeV and they give a small contribution (maximum 10%) in the total feeding of the low-lying states and as a consequence the uncertainties on Γ_{feed} for these states do not effect the final results.

The analysis of the results obtained in the experiments at 4.1 and 7.5 MeV end point energies with ^{116}Sn and ^{124}Sn allows us to conclude that the sensitivity of the measurements is quite high enough to get the total feeding of the low-lying states with a reasonable accuracy.

The estimates performed in the framework of this approach give $\langle \Gamma_{0_{\lambda}} / \Gamma_{\lambda} \rangle = 0.54$ for ^{116}Sn and $\langle \Gamma_{0_{\lambda}} / \Gamma_{\lambda} \rangle = 0.72$ in the case of ^{124}Sn over the energy region 5.0 to 7.4 MeV.

The estimated $\langle \Gamma_{0_{\lambda}} / \Gamma_{\lambda} \rangle$ values depend (but not so strongly) on the contribution of high-energy ground state transitions missed in our analysis (see Sec. V B). Including the missed transitions in the left part of Eq. (A7) leads to an increase of the average $\langle \Gamma_{0_{\lambda}} / \Gamma_{\lambda} \rangle$ and hence we have to consider the obtained value as a lower limit for this ratio. An additional 50% of missed ground state transition strength would increase the $\langle \Gamma_{0_{\lambda}} / \Gamma_{\lambda} \rangle$ for ^{116}Sn from 0.54 up to 0.64.

[1] A. Bohr and B.R. Mottelson, in *Nuclear Structure* (Benjamin, New York, 1975), Vol. 2.
[2] P. Axel, K. Min, and D. Sutton, *Phys. Rev. C* **2**, 689 (1970).
[3] A. Leprêtre, H. Heil, R. Bergère, P. Carlos, A. De Miniac, A. Veyssièrè, and K. Kernbach, *Nucl. Phys.* **A219**, 39 (1974).
[4] G. Bartholomew, E. D. Earle, A. J. Ferguson, J. W. Knowles, and M. A. Lone, *Adv. Nucl. Phys.* **7**, 229 (1973).
[5] R. Laszewski and P. Axel, *Phys. Rev. C* **19**, 342 (1979).
[6] R. Laszewski, *Phys. Rev. C* **34**, 1114 (1986).
[7] R. Alarcon, R. Laszewski, A. Nathan, and S. Hoblit, *Phys. Rev. C* **36**, 954 (1987).

[8] T. Chapuran, R. Vodhanel, and M. Brussel, *Phys. Rev. C* **22**, 1420 (1980).
[9] I. Iachello, Mini-Workshop on Low-Lying Magnetic and Electric Dipole Excitations in Nuclei, Darmstadt 1997 (unpublished).
[10] K. Heyde, C. D. Coster, B. Decroix, and A. Oros, *Phys. Rev. C* **57**, 1 (1988).
[11] P. V. Isacker, M. A. Nagarajan, and D. D. Warner, *Phys. Rev. C* **45**, 13 (1991).
[12] R. Herzberg, P. von Brentano, J. Eberth, J. Enders, R. Fischer, N. Huxel, T. Klemme, P. von Neumann-Cosel, N. Nicolay, N.

- Pietralla, V. Yu. Ponomarev, J. Reif, A. Richter, C. Schlegel, R. Schwenger, S. Skoda, H. G. Thomas, I. Wiedenhöver, G. Winter, and A. Zilges, *Phys. Lett. B* **390**, 49 (1997).
- [13] V. Soloviev, C. Stoyanov, and V. Voronov, *Nucl. Phys.* **A304**, 503 (1978).
- [14] K. Govaert, L. Govor, E. Jacobs, D. De Frenne, W. Mondelaers, K. Persyn, M. L. Yoneama, U. Kneissl, J. Margraf, H. H. Pitz, K. Huber, S. Lindenstruth, R. Stock, K. Heyde, A. Vdovin, and V. Yu. Ponomarev, *Phys. Lett. B* **335**, 113 (1994).
- [15] J. Bryssinck, L. Govor, D. Belic, F. Bauwens, O. Beck, P. von Brentano, D. De Frenne, T. Eckert, C. Fransen, K. Govaert, R.-D. Herzberg, E. Jacobs, U. Kneissl, H. Maser, A. Nord, N. Pietralla, H. H. Pitz, and V. Yu. Ponomarev, *International Conference on Nuclear Structure and Related Topics, Dubna, 1997* (to be published).
- [16] B. Mottelson, in *International Conference on Nuclear Structure*, edited by D.A. Bromley and E.W. Vogt (University of Toronto Press, Toronto, 1960), p. 525.
- [17] S. Raman, L. Fagg, and R. Hicks, *Electric and Magnetic Giant Resonances in Nuclei*, edited by J. Speth (World Scientific, Singapore, 1991), p. 355.
- [18] C. Djalali, N. Marty, M. Morlet, A. Wilis, J. C. Jourdain, N. Anantaraman, G. M. Crawley, A. Galonsky, and P. Kitching, *Nucl. Phys.* **A388**, 1 (1982).
- [19] R. Alarcon, R. Laszewski, and D. Dale, *Phys. Rev. C* **40**, 1097 (1989).
- [20] F. R. Metzger, *Prog. Nucl. Phys.* **7**, 53 (1959).
- [21] S. Skorka, *The Electromagnetic Interaction in Nuclear Spectroscopy*, edited by W.D. Hamilton (North-Holland, Amsterdam, 1975), p. 283.
- [22] U. Kneissl, H. Pitz, and A. Zilges, *Prog. Part. Nucl. Phys.* **37**, 349 (1996).
- [23] K. Govaert, W. Mondelaers, E. Jacobs, D. De Frenne, K. Persyn, S. Pommé, M. L. Yoneama, S. Lindenstruth, R. D. Heil, U. Kneissl, and H. H. Pitz, *Nucl. Instrum. Methods Phys. Res. A* **337**, 265 (1994).
- [24] F. Ajzenberg-Selove, *Nucl. Phys.* **A433**, 1 (1985).
- [25] F. Ajzenberg-Selove, *Nucl. Phys.* **A460**, 20 (1986).
- [26] U. Berg, H. Wolf, B. Schäfer, and K. Wienhard, *Nucl. Instrum. Methods* **129**, 155 (1975).
- [27] G. Audi and A. Wapstra, *Nucl. Phys.* **A565**, 66 (1993).
- [28] A. Jung, Ph.D. thesis, Giessen, 1992.
- [29] K. Govaert, Ph.D. thesis, Gent, 1996.
- [30] J. Blachot and G. Marguier, *Nucl. Data Sheets* **73**, 81 (1994).
- [31] T. Tamura, K. Miyano, and S. Ohya, *Nucl. Data Sheets* **41**, 413 (1984).
- [32] A. Demidov and I. Mikhailov, *Bull. Acad. Sci. USSR, Phys. Ser.* **54 (11)**, 41 (1990).
- [33] P. Endt, *At. Data Nucl. Data Tables* **26**, 47 (1981).
- [34] U. Berg, Habilitation thesis, Giessen, 1985.
- [35] F. Iachello, *Phys. Lett.* **160B**, 1 (1985).
- [36] T. Chapuran, R. Starr, R. Vodhanel, and M. Brussel, *Phys. Rev. C* **30**, 54 (1984).
- [37] V. Soloviev, *Theory of Atomic Nuclei: Quasiparticles and Phonons* (Institute of Physics Publishing, Bristol, 1992).
- [38] T. Marumori, M. Yamamura, and A. Tokunaga, *Prog. Theor. Phys.* **31**, 1009 (1964).
- [39] V. Voronov, D. T. Khoa, and V. Y. Ponomarev, *Bull. Acad. Sci. USSR, Phys. Ser.* **48**, 190 (1984).
- [40] F. Bauwens, J. Bryssinck, D. De Frenne, K. Govaert, L. Govor, J. Heyse, E. Jacobs, and W. Mondelaers, *International Conference on Nuclear Structure and Related Topics* [15].
- [41] A. Demidov and I. Mikhailov, *Topics in Atomic Science and Technology, Ser. Nucl. Const.* **4**, 24 (1990).
- [42] S. Raman, T. A. Walkiewicz, S. Kahane, E. T. Journey, J. Sa, Z. Gacsi, J. L. Weil, K. Allaart, G. Bonsignori, and J. F. Shriner Jr., *Phys. Rev. C* **43**, 521 (1991).